TÉCNICO LISBOA

Integration of a Combined Heat, Hydrogen and Power System at Sines Refinery Power Plant using Solid Oxide Fuel Cells

Catarina da Cunha Laboreiro Mendonça

Thesis to obtain the Master of Science Degree in

Chemical Engineering

Advisor(s)/Supervisor(s): Prof. Diogo Miguel Franco dos Santos (IST) Eng. António Ferreira dos Santos (Galp)

Examination Committee

Chairperson: Prof. Henrique Aníbal Santos de Matos
Advisor: Prof. Diogo Miguel Franco dos Santos
Members of the Committee: Eng. Hugo Coelho Santos

October 2021

Declaration

I declare that this document is an original work of my own authorship and it fulfills all the requirements of the Code of Conduct and Good Practices of the Universidade de Lisboa.

Declaração

Declaro que o presente documento é um trabalho original da minha autoria e que cumpre todos os requisitos do Código de Conduta e Boas Práticas da Universidade de Lisboa

Acknowledgments

First of all, I would like to thank my supervisors, professor Diogo Santos and Engineer António dos Santos, for their full support and availability throughout the development of my master's thesis, for their trust on my work and pushing me to the next level. To Engineer Hugo Santos, thank you for enlightening and help me along with the challenges this thesis had, always with great enthusiasm.

To my friends in Técnico, not enough words would express my dearest gratitude for their support, laughs and teamwork along these five years, however, Beatriz and Sofia, I know for a fact life was and is easier, lighter and happier with you around.

To Beatriz and Inês, thank you for all the good moments, the thoughtful advice and the undoubtful support since seventh grade until now and beyond.

To my parents and brother, my role models, who never questioned my capabilities even when I did, thank you for showing me how hard work is the best tool for success. Your love and support are my strength.

Lastly, to these five years in Técnico, which show me that "Success is not final, failure is not fatal: it is the courage to continue that counts" (Winston Churchill).

Abstract

On this thesis, the feasibility of a Combined Heat, Hydrogen and Power (CHHP) system to implement at Galp's refinery is studied, using Solid Oxide Fuel Cells (SOFC) as a clean power source. To evaluate its feasibility, this trigeneration system was simulated using Aspen Plus V11 software. Considering 10 kmol/h of fuel gas and 219.8 kmol/h of fresh air, 16.5 kg/h of hydrogen (99.999% purity) and 3 MMBtu/hr of heat were produced. Regarding the electrical power produced, it was determined by modelling the SOFC using the partial pressures of hydrogen, oxygen and water from Aspen Plus as input data and the result was 1.06 MW. Additionally, an economic analysis was included on this study to understand if the investment carried out would be viable. From this point of view, the production of high purity hydrogen presents a more significant impact on the profitibility of the trigeneration system than the electrical energy production, since the generated profit can compensate the investment performed on a 3 to 4 years period.

Keywords: Trigeneration; Solid Oxide Fuel Cell; High-Purity Hydrogen; Clean Power.

Resumo

Nesta tese, a aplicabilidade de um sistem combinado de produção de calor, hidrogénio e energia elétrica usando pilhas de combustível de óxido sólido foi estudada. O objetivo será a implementação deste sistema na Refinaria da Galp. Simulou-se o sistema de trigeração usando o *software Aspen Plus V11*. Considerando 10 kmol/h de fuel gas e 219,8 kmol/h de ar fresco, atingiu-se uma produção de 16,5 kg/h de hidrogénio com 99,999% de pureza e 3 MMBtu/h de calor. Relativamente à energia elétrica produzida (1,06 MW), esta foi determinada dimensionando a célula de combustível e recorrendo às pressões parciais da água, oxigénio e hidrogénio fornecidas pelo *software*. Realizou-se uma análise económica ao sistema, onde um período de 3 a 4 anos do projeto permite igualar o rendimento ao investimento efetuado caso haja uma sobreprodução acentuada de hidrogénio com elevado grau de pureza.

Keywords: Trigeração; Hidrogénio Puro; Pilha de Combustível de Óxido Sólido; Energia Limpa.

Contents

List of Tables

List of Figures

Acronyms

AFC Alkaline Fuel Cell.

AFL Anode Functional Layer.

ASC Anode Supported Cell.

BASE Beta Alumina Solid Electrolyte.

BoP Balance of Plant.

CCHP Combined Cooling, Heat and Power.

CEPCI Chemical Engineering Plant Cost Index.

CHHP Combined Heat, Hydrogen and Power.

CHP Combined Heat and Power.

CR Catalytic Reformer.

DMFC Direct Methanol Fuel Cell.

ESC Electrolyte Supported Cell.

FCH-JU Fuel Cells and Hydrogen Joint Undertaking.

GT Gas Turbine.

HP High Pressure.

HRSG Heat Recovery Steam Generator.

HTFC High Temperature Fuel Cell.

IST Instituto Superior Técnico.

IT Intermediate Temperature.

LPG Liquified Petroleum Gas.

LSCr Lanthanum Strontium Chromite.

LSM Lanthanum Strontium Manganate.

LT Low Temperature.

MCFC Molten Carbonate Fuel Cell.

MEA Membrane Electrode Assembly.

MIEC Mixed Ionic Electronic Conductor.

MSC Metal Supported Cell.

MW Mega Watt.

OCV Open Circuit Voltage.

ORC Organic Rankine Cycle.

ORR Oxygen Reduction Reaction.

PAFC Phosphoric Acid Fuel Cell.

PEM Proton Exhange Membrane.

PEMFC Proton Exhange Membrane Fuel Cell.

PSA Pressure Swing Adsorption.

REN Rede Elétrica Nacional.

SMR Steam Methane Reforming.

SOFC Solid Oxide Fuel Cell.

SOFCR Solid Oxide Fuel Cell Reformer.

SSOFC Symmetrical Solid Oxide Fuel Cell.

SSZ Scandia Stabilized Zirconia.

ST Steam Turbine.

TEC Thermal Expansion Coefficient.

TSO Trasmission System Operator.

WGS Water Gas Shift.

YSZ Yttria Stabilized Zirconia.

Chapter 1

Introduction

1.1 Context and Motivation

Exponential growth of the total population in the world and progress in civilization resulted in a massive demand for energy resources that are primarily reliant on fossil fuels. Nevertheless, as it is widely known, fossil fuels present several disadvantages, especially when applied in internal combustion engines where vast amounts of greenhouse gases are produced, resulting in a destructive effect on the environment [1]. Thus, it is crucial to develop advanced clean energy systems in order to switch from a fossil fuel-based economy to a new paradigm structure [2]. The hydrogen economy has been proposed as a possible method in which hydrogen plays as one of the main global energy carriers. It can be applied in fuel cells to generate power from an electrochemical reaction rather than combustion, producing only water and heat as byproducts, providing energy for transportation, buildings, and industry [3].

Fuel cell technologies are achieving a lot of attention through research and industry sectors due to their potential to provide long-term durability in clean energy to consumers, high energy conversion efficiencies, flexibility in design, and flexibility in fuel choice [4]. The fact that there is only one step involved (from chemical to electrical energy) comparatively to the multi-step (from chemical to thermal to mechanical to electrical energy) processes in combustion-based heat engines offers multiple advantages, especially from an environmental point of view. Additionally, in contrast to conventional battery materials, hydrogen and hydrocarbon fuels consumed in fuel cells contain a significant amount of chemical energy [5]. Fuel cells possess a static nature that reflects on a silent operation, while their implicit modularity grants for simple construction and adverse range of applications in portable, stationary, and transportation power generation [6]. Fuel cell technology can come as a solution to provide energy for rural areas with no access to the public grid, or a huge cost of wiring and transferring electricity is required. Applications with crucial secure electrical energy requirements such as continuous power supplies, power generation stations, and distributed systems can employ fuel cells as their source of energy. There are also some constraints related to this technology. For instance, contaminants in the gas streams and pulse demands deeply affect fuel cell's life span. Moreover, a lower power density per volume, less accessibility, and durability represent also challenges [5].

Each cell is composed of four main parts: anode, cathode, electrolyte, and the external circuit. There are multiple designs available for fuel cells yet, they all operate according to the same assumptions, the only difference is the chemical characteristics of the electrolyte [7]. In the majority of fuel cells, hydrogen is feeded to the anode where it is oxidized, producing electrons and hydrogen ions. Hydrogen ions flow through the acidic electrolyte while electrons are forced through an external circuit all the way to the cathode. At the cathode, electrons and hydrogen ions react with oxygen, producing water [6].

Anode:

$$2H_2 \rightarrow 4H^+ + 4e^- \tag{1.1}$$

Cathode:

$$O_2 + 4e^- + 4H^+ \rightarrow 2H_2O \tag{1.2}$$

The by-products of the global reaction in the fuel cell are water, heat and electrical work, as showed bellow [6]:

Overall:

$$2H_2 + O_2 \rightarrow 2H_2O + electricity + heat \tag{1.3}$$

It should be pointed that, according to the nature of the electrolyte, either protons or oxide ions are transported through an ion-conductor electron-insulating electrolyte [8]. Additionally, heat and water produced should be removed continuously in order to maintain an isothermal operation for ideal power generation [6].

Regarding the several types of fuel cells, these types include proton exchange membrane fuel cells (PEMFCs), direct methanol fuel cells (DMFCs), alkaline fuel cells (AFCs), molten carbonate fuel cells (MCFCs), phosphoric acid fuel cells (PAFCs) and solid oxide fuel cells SOFCs [1].

In PEMFCs, hydrogen is activated by a catalyst (Platinum or Platinum– Ruthenium supported in carbon), at the anode side, to form proton ions that flow through the membrane while electrons are forced to pass the external circuit and generate electricity. Electrons flows back to the cathode and react with oxygen and proton ions to form water [6, 5]. These reactions are described in 1.1 and 1.2.

PEMFCs are composed of bipolar plates and a membrane electrode assembly (MEA). The MEA comprises a dispersed catalyst layer, carbon cloth, or gas diffusion layer, which accesses the fuel uniformly and the membrane itself [5]. PEMFCs may be low temperature (60-80ºC) or high temperature (110-180ºC) fuel cells [6]. They are lightweight compact systems with fast start-up times, extended lifetime, and are less costly to manufacture [9, 10]. Its electrical efficiency is in the range of 40 and 50% and the output power can reach 250 kW. These types of fuel cells are frequently utilized in portable and stationary applications. Nevertheless, PEMFC systems are being successfully implemented in fuel cell vehicles due to their continuous electrical energy supply at a high level of efficiency and power density [5].

Direct methanol fuel cell (DMFC) use methanol as fuel, which is reformed into carbon dioxide (CO_2), in the anode. At the cathode, steam or water is produced using the oxygen available in air [5]. The reactions are displayed in equations 1.4 and 1.2 while the overall reaction is represented in 1.5.

Anode:

$$CH_3OH + H_2O \rightarrow CO_2 + 6H^+ + 6e^- \tag{1.4}$$

Overall reaction:

$$(3/2)O_2 + CH_3OH + H_2O \rightarrow 3H_2O + CO_2 \tag{1.5}$$

Methanol can be used in the form of vapor or liquid. Regarding cell voltage and power density, a vapor feed is a better option in contrast to a liquid feed. Nevertheless, it is associated with a lower lifetime, a higher temperature is demanded for fuel vaporization, and it can cause membrane dehydration. In consequence, a more complex and expensive reformer is used, and it is not convenient for portable applications. A crucial component in DMFCs is the Proton Exchange Membrane (PEM) which provides low penetrability, high proton conductivity, and high thermal and chemical stability for proper performance. Flemion from Asahi Chemical and Nafion from Dupont are the most used perfluorinated ion-exchange polymers used for DMFC. DMFC systems operate between ambient temperature and 110ºC and are usually ranked into active and passive. Active DMFCs comprise a methanol feed pump, CO_2 separa-

tor, fuel cell stack, methanol sensor, circulation pump, pump drivers, and controllers. Efficiency can be seriously increased if a pump is used for water circulation. They are usually implemented in control applications for quantities such as flow rate, concentration, and temperature. Meanwhile, in passive DMFC systems, methanol pumping equipment and external process for blowing air inside the cell are erased. Thus, oxygen is diffused into the cathode via the air-breathing feature of the cell. The same happens to methanol, using an integrated feed reservoir controlled by a concentration gradient between the anode and the reservoir. Passive systems are economical, simplistic, and effective in reducing substantially parasitic power loss and system volume [5].

The AFC uses an alkaline potassium hydroxide (KOH) electrolyte in a water-based solution to produce electricity. Hydroxyl ions flow through the electrolyte allowing a circuit to be established, and electrical energy can be generated. At the anode, hydrogen reacts with hydroxyl ions with a negative charge to release water and electrons [5]. This oxidation reaction is described in 1.6. At cathode, oxygen, and water combined and absorbed electrons to produce hydroxyl ions as demonstrated below, in equation 1.7

Anode:

$$2H_2 + 4OH^- \rightarrow 4H_2O + 4e^- \tag{1.6}$$

Cathode:

$$O_2 + 2H_2O + 4e^- \rightarrow 4OH^- \tag{1.7}$$

AFCs are considered low operating temperature fuel cells, working between 60 and 90 ºC, and use low-cost catalysts such as nickel. Their electrical efficiency is approximately 60%, and in Combined Heat and Power (CHP) systems, it increases to more than 80%. Output power can be up to 20 kW [11]. Nowadays, AFCs are implemented in submarines, boats, forklift trucks, and niche transportation applications [12]. They use hydrogen and pure oxygen as feed to produce portable water, heat and electricity sources. The water produced is very useful in space crafts and space shuttle fleets as potable water. However, these types of fuel cells can get easily poisoned with CO_2. The electrolyte absorbs CO_2 through the conversion of KOH to potassium carbonate and therefore poisons the fuel cell, which concerns researchers to discover a new substitute for KOH [13].

MCFCs are considered high-temperature fuel cells (600-700ºC) that use a molten carbonate salt mixture as electrolyte suspended in a porous, chemically inert ceramic matrix of beta alumina solid electrolyte (BASE) [5, 6]. In MCFC, at the anode, methane and water are converted to hydrogen, carbon monoxide, and carbon dioxide [5].

$$CH_4 + H_2O \rightarrow CO + 3H_2 \tag{1.8}$$

$$CO + H_2O \rightarrow CO_2 + H_2 \tag{1.9}$$

At the same time, hydrogen and carbon monoxide react and produce electrons, using carbonate ions available in the electrolyte, as displayed in equations 1.10 and 1.11.

$$H_2 + {CO_3}^{2-} \rightarrow H_2O + CO_2 + 2e^- \tag{1.10}$$

$$CO + {CO_3}^{2-} \rightarrow 2CO_2 + 2e^- \tag{1.11}$$

At the cathode, reduction takes between carbon dioxide and oxygen where the new carbonate ions

formed flow through the electrolyte to the anode [14].

$$(1/2)O_2 + CO_2 + 2e^- \rightarrow {CO_3}^{2-} \tag{1.12}$$

MCFCs, owing to their considerably high operating temperature, can directly employ hydrogen, carbon monoxide, natural gas, and propane as fuel and do not demand noble metals as catalysts. They are specially used for natural gas and coal-based power plants in electrical utility, industrial and military applications. Their major downside is the extended time needed to reach the operating temperature and generating power [14, 15].

PAFCs utilize carbon paper electrodes and a liquid phosphoric acid electrolyte. They are submitted to a temperature range of 150–220 ºC. Hydrogen ions flow from the anode to the cathode side and simultaneously electrons reach the cathode through an external circuit. At the cathode side, reaction between electrons, protons and oxygen takes place to form water and heat, with the presence of a platinum catalyst to accelerate the reactions, 1.1 and 1.2 [5].

The presence of CO_2 doesn't damage the electrolyte and cell performance therefore, PAFCs don't require pure oxygen for their operation. They use air as feed and can be operated with reformed fossil fuels. Nevertheless, employing air increases PAFC initial cost since it results in a significant reduction in the current density. Thus, PAFC is designed in a stack bipolar plate which improves electrode's area for more energy production. This expensive manufacturing cost is also a consequence of the need for finely dispersed platinum catalyst coating the electrodes. Nowadays, PAFC systems are commercially available with a capacity reaching 200 kW. Their electrical efficiency is between 40 and 50% and CHP efficiency around 85%. They are usually employed for on-site stationary applications [16, 17, 18].

SOFCs are considered high-temperature fuel cells (800-1000ºC) with a metallic oxide solid ceramic electrolyte [6]. Hydrocarbon fuels are reformed internally, generating a mixture of hydrogen and carbon monoxide, and air is used as the oxidant in the fuel cell [8]. Yttria stabilized zirconia (YSZ) is the most frequently used electrolyte for SOFCs due to its high chemical and thermal stability and pure ionic conductivity [19, 20]. Oxygen is reduced at the cathode, while fuel oxidation occurs at the anode (1.13,1.14 and 1.15). A porous anode facilitates fuel conduction and transportation of products away from the electrolyte and fuel electrode interfaces [21, 22].

Anode:

$$H_2 + O^{2-} \rightarrow H_2O + 2e^- \tag{1.13}$$

$$CO + O^{2-} \rightarrow CO_2 + 2e^- \tag{1.14}$$

Cathode:

$$O_2 + 4e^- \rightarrow 2O^{2-} \tag{1.15}$$

SOFCs are implemented in large scale distributed power generation systems with a power output in the range of MWs, but they can also be an option as local power generation systems for rural areas with no access to public grids. They present one of the highest overall efficiencies (70-80%) between the fuel cells since the heat produced is applied to generate more electricity by turning gas turbines. SOFC systems are modular and present flexibility in the choice of fuel with low noxious gas (NOx and SOx) emissions [5]. Additionally, there are no moving components in the fuel cell (except for balance of plant (BoP) components), noise and vibrations associated are practically non-existent [23]. However, their high operating temperature causes extended start-up and cooling-down times as well as various mechanical and chemical compatibility constraints which restrict the use of SOFCs. If the working temperature is reduced, SOFCs may be an interesting solution to change the energy production pattern [5].

One of the multiple applications fuel cells are incorporated in is the trigeneration concept - Combined Hydrogen, Heat and Power (CHHP). The most suitable candidates to be applied in CHHP are high-temperature fuel cells, MCFCs and SOFCs, which release enough heat during electrochemical reactions to efficiently produce hydrogen in order to be separated and purified for transportation purposes for instance. Both systems are among the High Temperature Fuel Cells (HTFCs) that present higher electrical efficiency and lower CO_2 emissions when in comparison with fossil fuel power plants [24]. Regarding stationary power plant applications, SOFC is the dominant technology since it has a relatively higher power density and is less corrosive than the MCFC, which due to the nature of the electrolyte (molten salt), can be lost throughout a long term operation [24, 25]. Additionally, this new concept focuses on producing useful power (electricity and heat) and hydrogen with a high efficiency associated. This can come as a solution for industries to achieve greater productivity and quality in their products and still manage to engage a more rational and sustainable use of primary energy resources.

In Portugal, there is a tight policy regarding CO_2 emissions, taxes are increasing exponentially, and incentives to search for greener technologies are becoming more predominant [26]. Galp is responsible for the largest hydrogen production and utilization in Portugal. Recently, it has joined the Hydrogen Council, an association of large companies and institutions worldwide that aspires to promote the development of hydrogen as the most competitive solution for the decarbonization of many sectors of the economy. Galp's large-scale projects are mainly directed to the production of green hydrogen from renewable energy and its association with the decarbonization of industrial processes and mobility or for injection into natural gas networks. These projects are included in the company's strategic objective of directing approximately 40% of its net annual investment to opportunities related to the energy transition, and that contribute to globally reduce CO_2 emissions [27]. In this manner, Trigeneration systems may be a huge opportunity to reduce not only primary energy consumption but also achieve economic benefits, increase electrical reliability, and produce a new feed of high purity hydrogen for different purposes.

1.2 Objectives and Structure of the Thesis

This work aims to evaluate the State-of-the-Art regarding solid oxide fuel cells and trigeneration systems, collect data in Sines refinery to assess the specific needs of the power plant, make a detailed analysis of the adequate proposal for trigeneration application, and provide an economic analysis considering the integration at Sines refinery.

Chapter 2

Galp's Framework

Galp's refinery, located in Sines, comprises four plants. Plants I, II, and III are responsible for producing Liquified Petroleum Gas (LPG), naphtha, gasoline, middle distillates, and fuel. Utilities demanded by these, such as steam, electrical energy, demineralized water, cooling water, fuel oil, among others, are produced in the fourth plant which is known as *Utilidades*. Herein, a Cogeneration system was implemented in 2009, comprising two recovery boilers equipped with an afterburner system (Heat Recovery Steam Generator - HRSG) and two Gas Turbines (GTs) to produce High Pressure (HP) steam and electrical energy, respectively, by burning natural gas [28]. The plant operates with an overall efficiency (steam + electric power) of 72% and is composed with the following equipment and functional systems [28]:

- Two natural gas turbines with a total power in continuous operation of 41 MW and an estimated electrical efficiency of 31.9%;
- Two boilers for recovering the energy contained in the exhaust gases from the turbines equipped with a post-combustion system using natural and fuel gas for the maximum unitary production of 125 ton/h of superheated steam at a pressure of 83 bar and 523ºC;
- Two final exhaustion chimneys with a height of 40 m relative to the ground;
- Two bypass chimneys, used to start and stop the turbines and/or in emergency situations.

Regarding auxiliary systems these include:

- High-voltage electrical system and transformers;
- Medium and low voltage electrical system;
- Fuel system;
- Compressed air system;
- Piping, ducts and mechanical connections system;
- Instrumentation, auxiliary control and data acquisition system;
- Fire protection system.

Focusing on the process of producing electricity and steam, it begins with the capture of ambient air in the gas turbines through highly efficient filters. Subsequently, the air is compressed in the turbine compressor until it reaches the pressure determined by its compression ratio. Natural gas is injected into

the turbines' combustion chamber at a pressure of around 25 bar and reacts with the air. The combustion gases at high temperature and pressure expand in the turbines, generating sufficient energy to drive the air compressor itself and the alternator coupled to the generator set. After expansion in the gas turbine, the exhaust gases with a temperature of around 550ºC are led to the respective recovery boiler. In the recovery boilers, equipped with an additional fuel burner system, heat is transmitted by convection between the hot combustion gases and the water/steam circulating inside the boiler tubes. The steam produced is subsequently superheated to around 520ºC and conducted to the Refinery's high pressure manifold, where it is distributed. The flash steam generated in the purge tank of each of the boilers is recovered and sent to the Refinery's low pressure steam line [28].

Overall, the electrical energy generated corresponds to 82 MWh (2×41 MWh) which is sell in the wholesale market with a Feed In Tariff. Electrical demand of Sines Refinery is supplied by conventional steam turbines and the remained consumption feed by an interconnection with Portuguese Trasmission System Operator (TSO), *Rede Elétrica Nacional* (REN). Nevertheless, for the GT's start-up, it is required an electrical energy consumption from the auxiliary equipment, which, afterward, is no longer needed since it begins to be auto consumed, meaning part of the energy produced is used to supply that equipment. Moreover, approximately 50% of the utility produced is injected into the Portuguese TSO (REN).

Therefore, studying the possibility of providing electrical energy for GTs auxiliary equipment could substantially improve the cogeneration system's efficiency since a more significant amount of electrical energy would be injected into REN, bringing economic benefits.

This thesis intends to evaluate the techno-economic feasibility of implementing a CHHP system integrated with a SOFC system fuelled with fuel gas. The main objectives are to attain an electrical power output of around 1.06 MW for GTs auxiliary equipment and produce hydrogen to supply refueling stations. In addition, reduce a considerable amount of CO_2 emissions with the SOFC system and the exploitation of the fuel gas, avoiding discharges on the flare.

Chapter 3

State-of-the-Art

The following literature review was submitted and published during the dissertation process [29].

3.1 Solid Oxide Fuel Cells

3.1.1 Fundamentals of SOFCs

Working Principles

SOFCs comprise porous electrodes separated by a dense ceramic electrolyte [1, 30]. Hydrogen and CO are fed into the anode of the fuel cell, and oxygen from the air, enters the cell through the cathode. On the anode side, H_2 and CO are oxidized and emit electrons that flow to the cathode, through an external circuit. After receiving electrons, O_2 undergoes a reduction reaction producing oxygen ions which are conducted through the ceramic electrolyte and react with fuel to produce H_2O and CO_2 in an exothermic chemical reaction that generates heat additionally [30, 31, 32]. Reactions are described in 1, equations 1.13, 1.14, 1.15.

Reforming natural gas or other hydrocarbon fuels to obtain the required hydrogen can be achieved within the fuel cell, excluding the requirement for an external reformer in contrast to the other types of fuel cells [30].

Cell design of SOFCs

The most common cell designs are anode-supported cells (ASC), and electrolyte-supported cells (ESC), however metal-supported cells (MSC) also play a role in the emerging market. The anode-supported cell technology is quite susceptible to RedOx cycling, known as repetitively coupled reduction and oxidation reactions, often involving oxygen and reactive oxygen species. Nevertheless, it is also the most common owing to high performance at low temperature, thanks to the dense thin electrolyte, while metal-supported cells should be the most stable [33]. Regarding electrolyte-supported cell, it is a robust cell

under RedOx conditions. Yet, as a consequence of the high ohmic loss in the thick electrolyte at temperatures between 700–800 ºC, a higher temperature is requested, which makes the impact of the faster reoxidation imperative [33, 34].

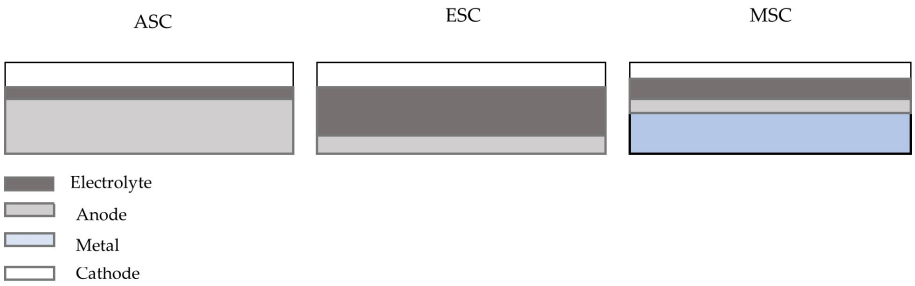

Figure 3.1: SOFC types:anode supported-cell (ASC), electrolyte-supported cell (ESC), and metal-supported cell (MSC).

Stack design of SOFCs

Planar design

In addition to two porous electrodes, separated by a dense layer (electrolyte), an assembling of many cells (stack) also comprises an interconnect and sealant - which can prevent the mixing of fuel and air [1]. The planar design is largely investigated since it can achieve higher power volume density, and it can be optimized to minimize reoxidation of the anode supported cell [35].

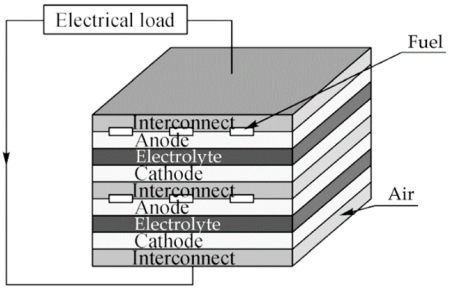

Figure 3.2: Planar SOFC design [1].

Monolithic design

This type of SOFC is based on a primary structure design comparable to that of a heat exchanger. The main structure contains a thin cell with the electrodes and electrolyte, plus interconnect and current collectors that are put together into a channeled structure. There are two distinct arrangements for this design, gas co-flow and gas crossflow [1, 35].

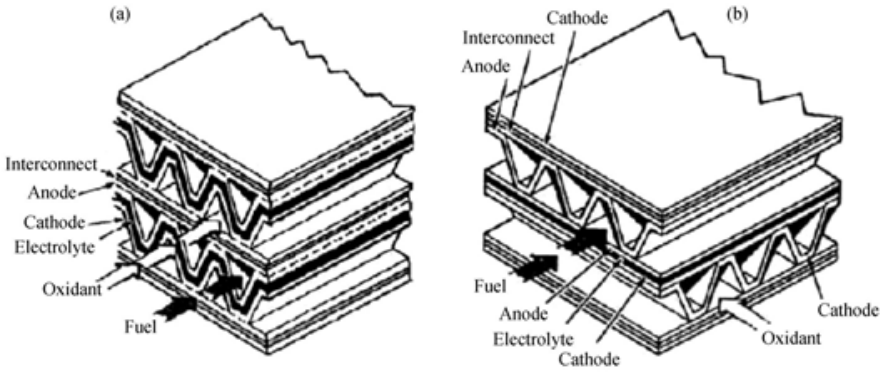

Figure 3.3: Monolithic SOFC design [1].

Tubular design

This configuration comprises a tubular support tube coated with the cathode in the core, the anode in the outside cell, and the electrolyte in between. The oxidant is introduced across the core of the support tube, while the fuel flows at the outside of this support tube [1]. This design can be sealless and is known to resist transients [35]. Nowadays, they are relegated to a niche existence due to the expensive manufacturing process, and high ohmic losses, which reduce the ionic conductivity of the electrolyte [34, 36].

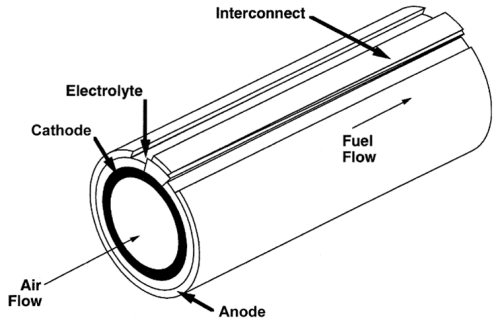

Figure 3.4: Tubular SOFC design [36].

Roll design

The arrangement and configuration in the roll design are prepared using a tape casting process: each element of the fuel cell is cast individually as an easily manipulated flexible tape. The components are laminated jointly and arranged to give the preferred geometry. Regarding fuel supply, it can be introduced in both anode and cathode (core) through stainless steel tubes [1, 37].

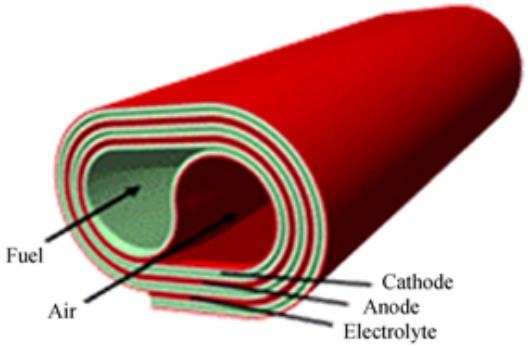

Figure 3.5: Roller SOFC design [37].

Fuel processing in SOFC

A huge variety of fuels such as natural gas, biogas, gasoline, kerosene can be applied in SOFCs adopting four different modes: external reforming, internal reforming, partial oxidation, and direct oxidation. The first three are reforming of fuels, wherein hydrocarbon fuels are converted into syngas (H_2 and CO) through steam reforming, dry/CO_2 reforming, partial catalytic oxidation, and oxidative steam reforming or auto-thermal reforming, and then electrochemically oxidized on the SOFC anode. The last one of these modes corresponds to the direct oxidation of fuels on the anode [38].

In external reforming, the endothermic steam reforming reaction and the fuel cell reaction are operated distinctly in different units with no direct heat transfer between both unit operations, while in internal reforming, these reactions are operated in a single unit [39]. There are two internal reforming modes: direct and indirect internal reforming. Indirect internal reforming physically divides the reforming process from the electrochemical process, recovering the cell-stack heat release. Alternatively, in the direct internal reforming, the hydrocarbon fuel–steam mixture is submitted directly into the anode segment, and the fuel is reformed on the nickel-based anode layer [39].

3.1.2 Material components of SOFCs

Electrolyte

An ideal SOFC electrolyte should have a high oxide ion conductivity, low electronic conductivity, low cost, and be environmentally benign. Good thermal and chemical stability towards the reactant environment and the electrode materials and closely matched thermal expansion coefficient (TEC) between electrodes and contacting components are also major features. Additionally, very thin layers can be fabricated, and a fully dense structure will enable to maximize conductivity and minimize reactant crossover. This reduces the internal cell resistance and prevents the mixing of the fuel and oxidant gas feeds

[8, 39, 40].

SOFCs can be classified into three categories according to types of conducting ions: oxygen-ion-conducting SOFCs, proton-conducting SOFCs, and mixed-ion-conducting SOFCs [9]. Due to these different conduction mechanisms, H_2O is generated on the anode in oxygen-ion-conducting SOFCs or on the cathode in proton-conducting SOFCs, whereas in the case of mixed-ion-conducting, it is formed on both anode and cathode [32].

Oxygen-ion-conducting electrolyte materials for SOFCs

The most traditional one is the oxygen ion transportation mode. Oxygen from the air is reduced to oxygen ions in the cathode, which is transported to the anode through the oxygen vacancy channel by the drive of concentration difference and potential difference [41]. The materials used in the electrolyte are yttria-stabilized zirconia (YSZ) and cerium oxide (CeO_2) stabilized by gadolinium (Gd) or Samarium (Sm) [42]. In addition to a good oxygen ion conductivity, these electrodes show good stability in both oxidizing and reducing atmospheres and are unreactive towards other components used in the SOFC. They are also abundant, rather low in cost, and strong, but easy to fabricate [8].

Yi and Anil produced anode-supported SOFCs with a thin film of YSZ as the electrolyte, and the maximum power density measured was 1.7Wcm^{-2} with hydrogen, 1.3 W cm^{-2} with CH_3OH, and 0.8 W cm^{-2} with alcohol–water (1:1 in volume) at 800 ºC, respectively. The study revealed that Tb-doped YSZ and Ti-doped YSZ could promote the peak power density up to 50% [43]. A range of dopant cations has been studied, including Y^{3+}, Eu^{3+}, Gd^{3+}, Yb^{3+}, Er^{3+}, Dy^{3+}, Sc^{3+}, Ca^{2+}, and Mg^{2+}. Scandia-stabilized zirconia (SSZ) gives the highest conductivity, even though Sc_2O_3 is more costly than Y_2O_3. Nevertheless, the amount applied in a thin supported electrolyte is smaller and therefore there is much interest in this electrolyte [40].

CeO_2-based electrolyte has shown several times a higher magnitude in oxygen ion conductivity than conventional YSZ electrolyte, especially at lower temperatures. However, Ce^{4+} is partially reduced to Ce^{3+} inside the electrolyte when there is a reducing atmosphere on the anode side, which not only causes the increase in electron conductivity in the electrolyte but also causes lattice expansion of the electrolyte. Consequently, this can generate a decrease in the open-circuit voltage of the cell and a decay in mechanical properties. Owing to these concerns, the performance of SOFCs with CeO_2-based electrolyte is quite inferior to the expected based on its conductivity, and its improved compatibility with mixed ionic-electronic conductor (MIEC) cathodes [41, 44]. Sm and Gd doped ceria were reported to be excellent ionic conductors for intermediate temperature SOFCs (nearly 6–7 times that of YSZ at 600 ºC), and outstanding compatibility with high-performance cathode materials, namely cobalt-containing perovskite oxide cathodes [45]. In addition, the effect of doping of alkaline earth oxides in ceria such as

CaO, SrO, MgO, and BaO was studied by Arai et al. They discovered that co-doping of ceria with two or more cations (alkaline earth and rare earth cations) improved the conductivity when compared with single-doped ceria in the air [46, 47].

Perovskite-type phases resulting from lanthanum gallate possess greater ionic conductivity than stabilized zirconia between 500 - 800 ℃. This is due to the substitution of La^{3+} by alkaline earth elements and/or integrating divalent metal cations, such as Mg^{2+}, into gallium sublattice, which increases the concentration of oxygen vacancies [48]. Introducing a small amount of cations with variable valences, such as cobalt, onto the gallium site, increases the ionic conductivity of LSGM ($La_{1-x}Sr_xGa_{1-y}Mg_yO_3$), and consequently a small increase in the electronic conductivity is reached [49]. Ishihara et al. have demonstrated that LSMG displays high ionic conductivity (comparable to that of GDC) and low electronic conductivity even at reduced partial oxygen pressure levels. This class of materials offers suitable performance at temperatures as low as 400 ºC [50], and have therefore be pointed as possible candidates for low and intermediate temperature SOFCs [51]. Nevertheless, LSGM is correlated with many inherent downsides, such as the expensive cost of the material, poor sinterability, and loss of Ga oxide throughout the sintering process when submitted to high temperatures. Interesting performance has been observed from electrolyte-supported, and thick film cells that have been manufactured using the optimized powders [44, 52].

Proton-conducting electrolyte materials for SOFCs

In the proton transportation mode, the hydrogen ions resulting from the oxidation reaction of hydrogen molecules that occurred in the anode are transferred to the cathode through the interface transfer based on the proposed ” swing model”. The proton-conducting material is an essential functional material with protons as charge carriers for the small diameter, lightweight, and reasonably high mobility of the particle. Amongst all the proton conductors as electrolytes for SOFCs, the $BaCeO_3$-based electrolytes display the highest proton conductivity [41].

Ito et al. set a 0.7-μm-thick $BaCe_{0.8}Y_{0.2}O_3$ thin electrolyte film on the Pd substrate and assembled a single cell that reached peak power densities of 900 and 1500 mW cm^{-2} at 400 and 600 ℃, respectively. Nonetheless, Pd is not appropriate for commercialization due to its high-cost [53]. $BaCeO_3$-based electrolytes are characterized by weak resistance to carbon dioxide and water corrosion, leading to lower proton conductivity, which leads to thermal expansion of the materials, and critically reduces the performance of SOFCs.

Another possible option as electrolyte material is $BaZrO_3$ which presents reasonably high stability in water or carbon dioxide atmosphere, and improved chemical and mechanical strength [41]. However, large-scale application is restricted due to its high grain boundary resistance and high sintering tempera-

ture. Improved proton conductivity is reached by reducing the grain boundary density for doped-$BaZrO_3$.

Mixed-ion-conducting electrolyte materials for SOFCs

Mixed-ion-conducting electrolytes result from the introduction of different types of electrolytes. These composite electrolytes allow for simultaneous diffusion of both oxygen ions and protons, increasing the ionic conductivity extensively. Usually, they comprise ceria-based carbonate composite electrolyte, ceria-based tungstate complex electrolyte, among others. It is stated that the total ionic conductivity of the composite material is higher than the total of each raw material. This means that the behavior of the composite material changes and stimulates the ionic conduction mechanism, enhancing the ionic conductivity. The composite electrolyte consists of two or more materials with distinct charge conduction characteristics, mostly including oxides and salts. These composite materials possess a high capability of conducting charges, and the ions conductivity can reach 0.01–1 S cm^{-1} at 400–600 ℃, which is significantly higher than the achieved from typical single-phase electrolyte materials [41].

Fabrication methods for electrolytes

To produce an intermediate temperature SOFC with relatively high performance, bilayering can be an interesting approach. Bilayered systems take into account two electrolyte layers to overcome the disadvantages associated with the single electrolyte layer. This type of strategy can lead to a synergistic effect to surpass the individual drawbacks and improve power performance for a prolonged period. Nevertheless, it also faces challenges, such as shrinkage compatibility, TEC compatibility, and possible interdiffusion between two components, which should be addressed [45]. Producing thin films minimizes ohmic losses in situations where the ionic conductivity at low temperatures is not sufficiently high. The most commonly used techniques to achieve this are atomic layer deposition, chemical vapor deposition, physical vapor deposition, pulsed laser deposition, atmospheric plasma spraying, and sol-gel [54].

Interconnect

The interconnect (also referred to as bipolar plate) in planar fuel cells has the vital role of separating the oxidant and the reducing fuel atmosphere, collecting the current from the electrodes, conducting the electrical current between adjacent cells, distributing reactant gas evenly across the face of each electrode and offering mechanical support to the cell, and stack structure [55]. The component must have a high electronic conductivity in both oxidizing and reducing atmospheres; low contact resistance with the electrodes; good thermal conductivity; very low permeability to reactant gases; and must not react with any of the other components at the high operating temperatures [8, 40].

The only proper material for interconnects in high-temperature SOFCs was alkaline-earth doped

$LaCrO_3$ or other Cr-containing perovskites [56]. Nevertheless, high-temperature metallic alloys are becoming suitable candidates and present considerable advantages. These are related to lower cost, the fact that they are genuinely electronic conductors and oxide ion insulators, and fabrication is trustworthy when compared to the ceramic ones [57, 58].

One potential alloy is the Cr-based oxide dispersed strengthened alloy, Cr-5Fe-Y_2O_3, known as Ducrolloy [59]. It exhibits excellent oxidation resistance along with a TEC that matches other adjacent SOFC materials. Nevertheless, one of the disadvantages of Ducrolloy is that excess Cr_2O_3-scales cause inadequately high area-specific resistance after oxidation at 1000 ºC for 75 h. Additionally, the current inaccessibility of a simplified fabrication process and high processing costs make this alloy unsuitable for application [60]. Ferritic stainless steel, a type of Fe-Cr-based alloy, when doped with optimum Cr-content (17%–25%), forms continuous C_2O_3-scales which renders excellent oxidation resistance and is considered the alloy with the most potential due to its economic feasibility and good TEC matching the other SOFC components [61, 62, 63].

Anode

The anode performs the electro-oxidation of the fuel by catalyzing the reaction and facilitating fuel access and product removal. Therefore, the anode material should be chemically compatible, thermally stable, highly (ionic, electronic) conductive, with a highly porous and organized structure, and fine particle size [1].

Due to SOFC's elevated working temperature and the reducing nature of the anode, only cobalt, nickel, and noble metals are possible candidates as materials for this component. The vast majority of SOFCs have a nickel anode due to its low cost when compared to the other options [8]. For the porous structure, nickel is dispersed with the solid electrolyte material to form a cermet (a composite of ceramic and metal), which keeps the porosity by avoiding sintering of the nickel particles throughout the operation and also provides the anode with a TEC similar to that of the solid electrolyte [8]. Moreover, this microstructure is optimized to have a fully percolated metallic component that allows conduction of electrons through the structure while optimizing the amount of active triple phase boundary (TPB), known as the interface at which the electronic and ionic conducting phases co-exist with the open pore containing fuel and where the reaction occurs in most cermets [40]. As it has been widely discussed, reducing the operating temperature continues to be one of the biggest obstacles towards SOFCs commercialization, as it also reduces the electrode materials' catalytic activity and the ionic conductivity of the electrolyte [60]. Hence, the latest studies to address this problem and improve the anode performance are discussed, dividing the anode materials into two groups: nickel-based cermet and perovskite-based

anodes [54].

Ni-based cermet

A high anode performance at low temperatures can be reached by introducing an anode functional layer (AFL). The interfacial resistance of the anode-supported SOFCs usually becomes prevailing at the intermediate temperature range. Given that the quality of the anode highly affects the cell performance, the AFL layer is usually characterized by a fine grain structure (to favor increasing TPB length). Wang et al. produced continuous-graded AFL via an electrophoretic co-deposition route and observed an increase in the TPB length and the consequent expansion of the area for electrochemical reactions on the anode [64]. Hyun and coworkers recently developed NiO-YSZ nano-composite materials for AFL, which showed high performance in Ni-YSZ-based cells [54, 65].

Ni-based cermets reveal some drawbacks such as low tolerance to the sulfur that exists naturally in fuels, to carbon, except if a considerable amount of steam is added to reform the fuel, and nickel coarsening along with inferior volume stability upon redox cycling [54, 66].

Perovskite oxides

Perovskite oxides in SOFC tend to exhibit simultaneously high oxygen ionic and electronic conductivities. This property is typical of MIECs. These MIEC perovskites have been studied as alternative ceramic anode materials. They present much larger areas of TPBs, leading to a better anodic performance relative to its electronic or ionic conducting perovskite counterpart. MIEC perovskite oxide is an appealing next-generation SOFC anode component since it has active sites that promote the activation of C-H bonds for hydrocarbon oxidation, which can be enhanced by adjusting the concentration of oxygen vacancies and their mobility to mitigate the carbon coking [67].

The strontium doped lanthanum chromite (LSCr) single perovskites have been a focus of study and characterization as SOFC anode materials over the past decade. LSCrM is one of the most known perovskites that displays high-temperature stability and good resistance to carbon deposits. It also shows redox stability when fueled under oxidizing and reducing environments, which allows its application as electrodes in symmetrical SOFC (SSOFC). Though LSCr-based perovskites have rather low electrical conductivity in reducing atmosphere, therefore showing weaker electrochemical reaction kinetics than Ni-YSZ [67]. Producing composite with redox-active transition metals such as Cu and Ni and changing the chemical composition of conventional LSCr-based anode are possible solutions to enhance catalytic activities and improve the electrical conductivity of these LSCr-based single perovskites [68].

Cathode

Cathodes in SOFCs have multiple roles within the cell: reduction of molecular oxygen, transport of charged species to the electrolyte, and supply of electrical current for the oxygen reduction reaction (ORR) [40]. Thus, the material used in SOFCs as cathode should be highly electronic conductive, chemically compatible, and thermally stable; highly porous, should not show any tendency to react with the electrolyte; easy to process and reliable manufacturing cost [1, 8, 69, 70]. Electrode materials are limited to noble metals or oxides with sufficiently high electronic conductivity due to the elevated operating temperature. As noble metals are excluded for economic reasons, oxides are exclusively used [8]. Perovskite materials with lanthanum manganite composition doped with rare earth elements, such as Co, Ce, or Sr, are commonly utilized [69, 70, 71, 72]. They provide a good matching in terms of thermo-mechanical performance with the electrolyte and, additionally, these materials are MIECs. Strontium-doped lanthanum manganite ($La_{1-x}Sr_xMnO_3$, LSM), is the most utilized cathode material for zirconia-based SOFCs.

$LaMnO_3$ is a perovskite material with intrinsic p-type conductivity, the oxygen stoichiometry of which at high temperature is a function of the oxygen partial pressure, having an oxygen excess in an oxidizing environment, whereas becoming oxygen deficient in reducing atmosphere. This results from the formation of cation vacancies, and hence the conductivity can be enhanced using a lower valence ion as a dopant for either the A or B sites, which can be stated through the formula ABO_3. A-site cations consist of alkaline or rare earth metal elements, such as La, Sr, or Ba, while B-site cations are 3d, 4d, or 5d transition metal elements, such as Mn, Fe, and/or Co. Moreover, $LaMnO_3$ is usually manufactured with lanthanum deficiency to avoid the formation of La_2O_3, which can lead the cathode layer to collapse through hydration to $La(OH)_3$ [73, 74, 75].

To enhance cathode performance at low temperatures, different approaches, such as doping, multiphase/composite cathodes, and nanostructured cathode fabrication by infiltration techniques or in situ exsolution, have been investigated [40, 54].

Cathodes on oxygen-ion-conducting electrolyte

Perovskite-type MIECs, have been applied in Intermnediate Temperature (IT) and Low Temperature (LT) SOFCs to increase the active sites to the whole cathode surface. Cobalt-containing perovskite oxides, namely $Ba_{1-x}Sr_xCo_yFe_{1-y}\ O_{3-\delta}$ (BSCF), $La_{1-x}Sr_xCoO_{3-\delta}$ (LSC), $La_{1-x}Sr_xCo_{1-y}Fe_yO_{3-\delta}$ (LSCF), and $Sm_{1-x}Sr_xCoO_{3-\delta}$ (SSC), are of particular importance. These oxides have MIEC and ORR activity related to Co(III)/Co(IV) transition [76]. However, their large-scale application raises some doubts as the flexible Co(III)/ Co(IV) redox behavior displays multiple technical concerns, such as low chemical stability, high TEC, and high reactivity with zirconium-based electrolyte [77].

Double perovskite cathodes have also been studied due to their faster rate of surface oxygen exchange and diffusion, higher electrical conductivity, and superior electrochemical performance than single perovskite cathode materials. He et al. verified that Sn-doped $Sr_2Fe_{1.5}Mo_{0.5-x}Sn_xO_{6-\delta}$ (x = 0, 0.1, 0.3, and 0.5) lead to low average formation energy and the increase in the oxygen vacancies concentration, which enhances the ORR performance, namely the surface exchange and bulk diffusion processes [78].

Cathodes on proton-ion-conducting electrolyte

Recent work suggests the application of $BaZr_{0.1}Co_{0.4}Fe_{0.4}Y_{0.1}O_3$ as a triple-conducting cathode on BZCYYb proton-conducting electrolyte [79]. The high content of Co and Fe (transition metals) in this material is the reason for its high catalytic activity and electronic conductivity. Y doping also enhanced the concentration of oxygen vacancies, creating its triple conducting function [61].

Composite cathodes

Composite cathodes have been extensively investigated to increase the cathodic performance by introducing a second phase into the electrode matrix to produce composite electrodes. Because of this second phase, the electrochemical reaction zone of ORR expands and minimizes the thermal and mechanical incompatibility between electrode and electrolyte. $Nd_{0.5}Sr_{0.5}Fe_{0.8}Cu_{0.2}O_{3-\delta}$-$Sm_{0.2}Ce_{0.8}O_{1.9}$ composite cathode with 40 wt.% $Sm_{0.2}Ce_{0.8}O_{1.9}$ component displayed stable performance for 370 h at 700 ºC without any substantial variation in the polarization resistance performance [78].

3.1.3 SOFC applications

As mentioned above, SOFCs are one of the most efficient and environmentally friendly technologies available for power generation [13]. There are three main applications of SOFCs related to this field: combined cycle power plant, cogeneration/trigeneration, and residential applications. SOFC are still not quite suitable for portable applications and transportation, as mentioned before, due to their high operating temperature, which leads to long start-up and cool-down times [39].

Combined gas turbine (GT) power system with SOFC

One of the main concerns regarding a conventional GT plant is associated with thermal efficiency since it has considerable losses related to the high irreversibility inside the combustion chamber. This can be improved if direct contact between air and fuel is prevented, as it occurs in fuel cells. A fuel cell–GT hybrid system has a higher energy conversion efficiency, low environmental pollution, and possible use of renewable energy sources as fuel. Although the thermal efficiency depends upon the cycle configuration

and layout of the hybrid system, such as a pressurized SOFC–GT combined cycle or a recuperated GT integrated with SOFC, an efficiency until 60% can be reached using the integrated cycle [39]. There are two different ways that gas turbines can be connected to the SOFC: indirect and direct integrations (fig. 3.6).

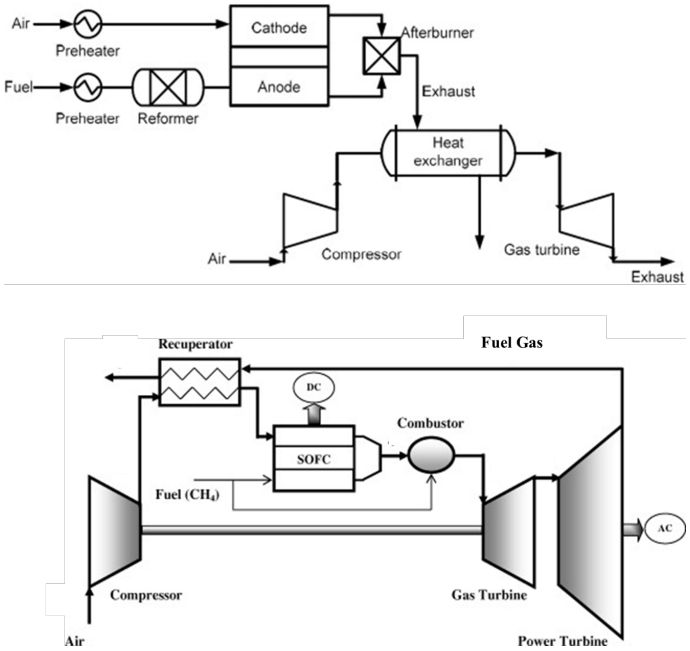

Figure 3.6: Indirect (top) and direct (bottom) combined gas turbine power plant with SOFC [39].

In the indirect SOFC–GT hybrid system, the combustor of the gas turbine is substituted with a heat exchanger in which air from the compressor is heated by the fuel cell exhaust (thermal energy) [39]. In contrast, in the direct SOFC–GT hybrid system, pressurized air from the compressor is preheated by the exhaust gas from the power turbine before entering the cathode side of the SOFC while fuel flows into the anode side. The outlet air from the cathode is utilized to burn the residual hydrogen, carbon dioxide, and methane in the anode outlet gas. The products of the chemical reaction are very lean; thus, supplying a fuel injection into the combustion chamber stabilizes the combustion. The resulting fuel gas is expanded in the turbine and preheats the compressor outlet air in the heat exchanger [39].

One disadvantage related to SOFC–GT system is the start-up time, which is much longer than in a GT conventional plant. Furthermore, in this system SOFC stacks need be pressurized in an extremely large vessel. This practical constraint is reduced in hybrid SOFC Steam Turbine (ST) systems since stacks operate under atmospheric pressure [80].

SOFC integrated with Rankine cycle

The scheme represented in fig. 3.7 consists of a hybrid system with a SOFC on top of a steam turbine [80]. If the operating temperature of SOFC stacks is reduced to an intermediate value, then the combination of SOFC–ST hybrid systems would be more appealing than the SOFC–GT systems. Not only, the material cost for the SOFC stacks is decreased, but also many problems associated with the BoP components are diminished [39]. A desulfurization reactor and pre-reformer are fitted in the plant. The sulfur contained in the fuel is removed in a desulfurization reactor, whereas the pre-reformer is responsible for breaking down heavier hydrocarbons. The pre-treated fuel then enters the anode compartment of the SOFC. After passing the SOFC stacks, the remaining fuels enter the burner, with the resulting exhaust gases being utilized to produce steam in a heat recovery steam generator through a Rankine cycle. This system can achieve a cycle efficiency of up to 67% [80].

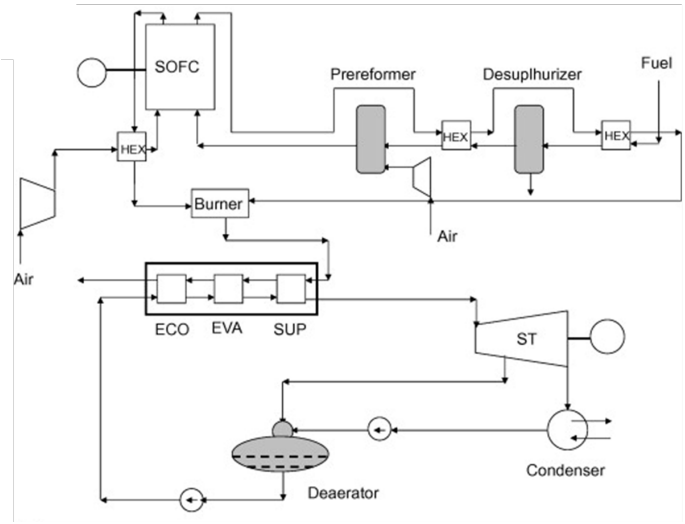

Figure 3.7: Combined SOFC–ST cycle plant with CPO reformer [80].

Cogeneration with SOFC

The heat rejected to the surrounding water or air in the conversion process is one of the major sources of loss owing to the intrinsic limitations of the different thermodynamic cycles used in power generation. Cogeneration or Combined heat and power (CHP) is identified as the sequential generation of two different forms of useful energy, usually mechanical and thermal energy, from a single primary energy source. SOFC's high-temperature exhaust gas can be employed for heating purposes, such as preheaters and reformers, to preheat the air before it arrives at the combustion chamber or it may be utilized to produce steam in a Rankine cycle, as seen above [39]. Chan et al. investigated SOFC power systems supplied by two different fuels: hydrogen and methane. The hydrogen-fed SOFC system consisted of two preheaters, a SOFC stack, and an afterburner where the unreacted fuel from SOFC was burnt and the heat

generated was provided to the reformer, vaporizer, and preheater. In contrast, the methane-fed SOFC system was somewhat more complex. It comprised a mixer, a vaporizer, two preheaters, an external reformer, a SOFC stack, and an afterburner. By comparing the two systems, the use of methane as fuel can provide higher efficiency than using pure hydrogen [81].

Trigeneration with SOFC

Trigeneration, defined as combined cooling, heating, and power (CCHP), is currently a promising technology for efficient and clean energy production. It uses in the best way possible the chemical energy of the fuel to generate electricity and heat from the exhaust. Simultaneously, cooling can be generated from absorption or desiccant cooling, consequently reducing the use of electricity in a traditional air conditioning unit [39]. This application will be revised in further detail in Section 3.2.

3.1.4 Latest projects and developments

There has been a huge effort from companies and governments to improve SOFC technology to achieve its full commercialization and mass production. The latest accomplishments on this matter are discussed in further detail.

Kyocera

Kyocera is a Japanese company that started developing miniaturized SOFC technologies in 1985. In 2011, the company began mass production of SOFC cell stacks and achieved further miniaturization with its 3rd generation product, attaining ca. 90 000 hours of continuous operation, 360 operation cycles (operated at 700 ºC in hydrogen/air conditions), and a power output of 700 W. These SOFCs are finding application both in households and in small businesses, such as restaurants and convenience stores [82]. In 2017, Kyocera Corporation announced the first 3 kW SOFC for institutional cogeneration using 700 W cell stacks. The system uses Kyocera's ceramic technologies and city gas as fuel to provide 52% generation efficiency and overall efficiency of 90% with exhaust heat recovery [83].

Bloom Energy

Bloom Energy (Silicon Valley energy startup) was founded in 2001 by Professor K.R. Sridhar, who had been working for NASA on the development of an electrolyzer powered by a solar panel to produce fuel and oxygen that would help support life on Mars [84].

Bloom Energy products are mainly stacks of planar electrolyte-supported fuel cells fabricated with metals sprayed on ceramic supports. Their SOFC systems currently possess up to 65% (LHV) net electrical efficiencies. The company focused on improving the size of their systems continuously in the last years, presently developing the ”Energy Server 5” with an electrical power output of 200-300 kW and the possibility of being combined to form a wider system owing to its modularity. These servers comprise 1 kW electricity stacks, coined as ’Bloom Boxes’, which consist of 40 cells of 25 W electricity each, fed with natural gas or biogas [85].

Bloom Energy had a huge impact on SOFC commercialization. In 2018, it sold 80.9 MW of SOFC systems, which can be compared to a total market of ca. 91 MW [85]. In the USA, it has provided fuel cell power generation systems for a considerable number of Walmart stores and several size units for companies, such as Apple, ATT, IKEA, Disney Pixar Animation Studios and Morgan Stanley [86].

FCH-JU

In Europe, the Fuel Cells and Hydrogen Joint Undertaking (FCH-JU) is a public-private partnership established to support research, technological development, and demonstration activities in the field of fuel cells and hydrogen energy technologies as an instrument in reaching a carbon-free energy system [87].

One of the projects included in FCH-JU was Demosofc, the first industrial size SOFC installation fed by biogas in Europe. It was installed in a municipal wastewater treatment plant of Collegno (Turin, IT). Here, the biogas resulted from sludge, a by-product of the water treatment process. The cogeneration system comprising SOFCs was composed of 3 modules, able to produce 58 kW AC each. The installed power covered a total of 174 kW, capable of delivering 30% of the plant’s electrical needs. Thermal recovery from the exhaust was employed to partially cover the anaerobic digester thermal load [88].

3.2 Trigeneration

Although trigeneration systems are commonly combined with internal combustion engines or GTs, fuel cells and Rankine Cycles, have also become promising technologies. Since the SOFC was the type of fuel cell chosen for this thesis, state of the art regarding trigeneration will be focused on using this fuel cell as a power generating unit.

The combination of SOFC based trigeneration systems can be established in multiple design methods. The most common one corresponds to plants that simultaneously provide electricity, cooling, and heating (CCHP). Nevertheless, there has been a growing interest in the development of trigeneration

systems that could produce other co-products, such as hydrogen (CHHP) [89].

3.2.1 Combined Cooling, Heating and Power (CCHP)

Regarding combined cooling, heat, and power system (CCHP), it can produce significant amounts of energy and reduce substantially CO_2 emissions when compared with the isolated generation of cooling, heat, and power [90, 91]. Besides the heat processes, waste heat is employed to produce cooling either by thermally driven heat pumps or desiccant systems [92]. Figure 3.8 shows the typical configuration of a trigeneration system. However, the hot water produced by a SOFC tends to be scarce to be applied in the heat exchanger and the absorption chiller thus, an Organic Rankine cycle (ORC), or an afterburner, or boiler is needed [93, 94, 95, 96, 97].

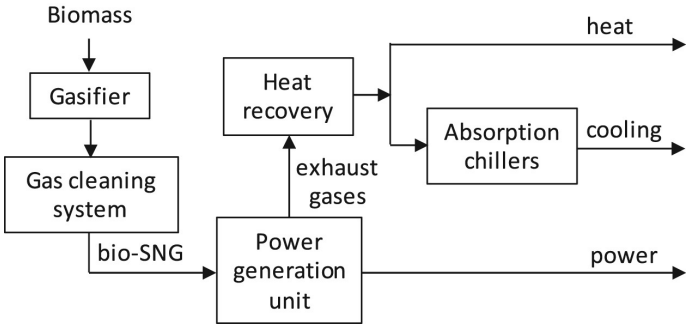

Figure 3.8: Diagram of CCHP system [97].

A SOFC-GT combined cycle plant was proposed by Burer et al. [98], comprising a heat pump to produce heating, a compression chiller, and an absorption chiller to produce cooling, and an additional gas boiler (for when the heating needed surpassed the one provided by the heat pump). The main goal of the plant was to fulfill heating and cooling demands, excess power produced by the SOFC-GT system was considered a by-product of the system. This system could provide heating for air conditioning, domestic hot water, and cooling effects for summer and mid-season for residential buildings within 20 years.

Moreover, Al-Sulaiman et al. [99] also suggested a new concept for SOFC based trigeneration. The system involves a SOFC, ORC, a heating process, and a single-effect absorption chiller. Waste heat from the SOFC is employed to heat the organic fluid (n-octane) in the ORC, whereas waste heat from the ORC produces steam in the heating process and cooling through a single-effect absorption chiller. Afterward, Al-Sulaiman et al. [100] proposed two other trigeneration systems, one biomass-based and the other solar-based, and compare their performances with that of the SOFC-trigeneration system. The study proves that the SOFC-trigeneration system has the highest electrical efficiency among the three systems. Regarding CO_2 emissions in kg per MWh of electrical energy, this study shows that these are relevant in the case of biomass-trigeneration and SOFC-trigeneration systems. Though, by considering

the emissions per MWh of trigeneration, those values reduce to less than one-fourth.

Yu et al. [101] considered a trigeneration system integrating a SOFC system with a double-effect water/lithium bromide absorption chiller. The exhaust gas produced in the SOFC passes through a heat recovery steam generator (HRSG), generating saturated steam used to drive a double-effect absorption chiller. Otherwise, the flue gas can enter a heat exchanger and produce hot water for distributed heating.

Weber et al. carried out detailed CO_2 emission and cost analyses of a trigeneration system based on a SOFC primary mover in an office building and found that CO_2 emissions were decreased by 30% at a cost growth of 70% compared with a conventional system [102].

Unfortunately, trigeneration is not quite spread worldwide owing to several motives. For example, investment costs tend to increase substantially with more complex equipment, and cold climate conditions are not extensively required, especially in developed countries, making such technology not that much appealing. Nevertheless, systems that demand comparable amounts of heat, cold, and electricity, for example, supermarkets, may favor CCHP. In addition, CCHP may be a compelling solution to fit buildings or complexes where constant electrical, heating and cooling supplies are required [103].

3.2.2 Combined Heat, Hydrogen and Power (CHHP)

The production of hydrogen, electricity, and heat can provide multiple advantages compared to simple cogeneration systems.

Hemmes et al. [104]. introduced a new concept for producing power, heat, and hydrogen using high-temperature fuel cells. The main goal is to extract hydrogen throughout electricity production. Separating hydrogen from the exhaust gas is possible, yet only at a small scale in contrast with the conventional hydrogen production using the steam methane reforming process in oil refineries. The authors [104] recommend implementing Pressure Swing Adsorption (PSA) technology with the further improvement of hydrogen membranes.

Becker et al. [105] also developed a CHHP system where the hydrogen produced can be used as PEM fuel cell-powered vehicles. PSA and Electrochemical Hydrogen Separation (EHS) are employed as two possible processes to purify and recover the hydrogen from the SOFC exhaust anode gas. Part of the anode-off gas stream is recycled, and the remaining part is cooled to 300ºC, favorable for the water gas shift reactor, with the intention to increase hydrogen production before entering the EHS or PSA units.

Fernandes et al. [106] considered a CHHP system where the hydrogen produced was also for fuel cell vehicle applications. Four system designs were taken into account with distinct reforming technologies: the catalytic reformer(CR) and a SOFC operating as a reformer (SOFCR), each with or without

carbon capture and storage. Additionally, as demonstrated in Fig.3.9, two operation modes were analyzed. In the first mode, the fuel cell as the electrical power source for a vehicle is considered to produce also water, whereas, in the pump mode, hydrogen is compressed and transferred to the vehicle's fuel tank. The study concludes that the SOFCR unit remarkably decreases the exergy destruction resulting in an improvement of efficiency over 20% when compared to CR-based system designs. The trigeneration exergy efficiency (mobility, electricity, and heat) is nearly 60% in SOFCR-based system.

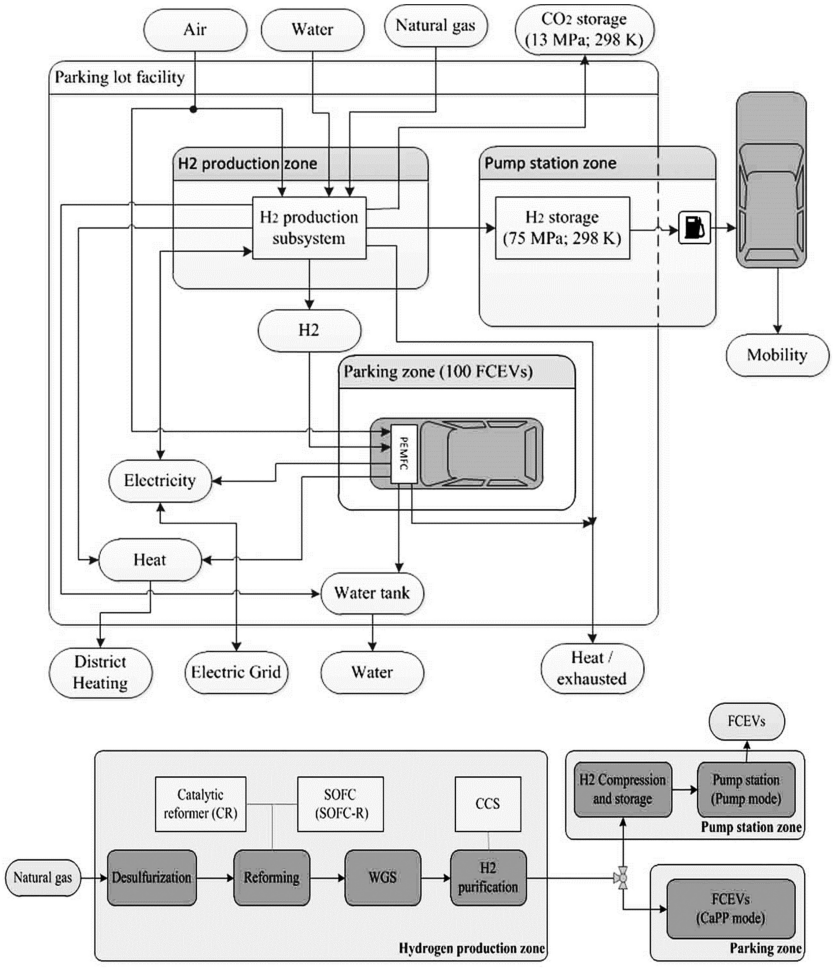

Figure 3.9: Trigeneration system and process path for hydrogen production [106].

In conclusion, combining a trigeneration plant with fueling stations for fuel cell vehicles allows using lower-scale (250–350 kg day^{-1}) hydrogen production. It leverages the capital investment among all co-products, thus decreasing the unit cost of hydrogen and offering a likely promising transition pathway towards a hydrogen economy [105].

Chapter 4

Aspen Implementation

4.1 Assumptions for Process Simulation

The feasibility of a CHHP system was tested in the process simulation software widely known as Aspen Plus V11. In order to fully comprehend how this software was developed, certain assumptions should be highlighted.

Starting with the SOFC conditions, it was established that it would be employed the model developed by Bloom Energy since it is one of the most mature technologies in the market. The Bloom Energy Server ES5-250 kW, was the technology chosen due to the availability of the information. This server is built up with 1 kW electricity stacks, labeled as 'Bloom Boxes', which are composed of 40 cells of 25 W of electricity each, operating at 850ºC [85, 107]. The output voltage of each cell is 0.8V DC [108]. According to Bloom's patent description, the electrolyte corresponds to SSZ. The anode and cathode are made from special inks that coat the electrolyte. The anode side is coated with a green nickel oxide-based ink, and the cathode side is coated with black ink (LSM) [109].

Regarding choosing the proper thermodynamic model for this simulation, in oil, gas, and petrochemical applications, the Peng-Robison property package is commonly recommended [110].

The following assumptions are made in this simulation process [111]:

- Steady-state
- Ideal gas model
- Reactions are in a chemical equilibrium condition due to a sufficient amount of time.
- The pressure drop in all equipment is ignored.
- Only H_2 is involved in the electrochemical reaction in the anode.

- The values of consumed H_2 in the electrochemical reaction is considered as the input of the model.
- The amount of consumed O_2 in the electrochemical reaction is considered to be a known input.
- Pure oxygen is provided in the cathode.

4.2 Input Auxiliary Calculations

In order to fulfill the input requested by Aspen Plus V11 software, the flow rates of each reactant must be determined.

As mentioned before, in a SOFC, hydrogen reacts with oxygen producing water, heat, and electrical current. The fuel provided by Galp's Refinery corresponds to fuel gas with the composition presented in table 4.1. This fuel gas will be submitted to a steam reforming process inside the fuel cell, producing hydrogen required for the electrochemical reaction.

Table 4.1: Molar composition of the fuel gas provided by Sine's Refinery, Galp.

Component	Composition (mol%)
H_2	40.8
CH_4	33.4
C_2H_6	12.8
C_3H_8	13.0

These values were obtained through chromatography and represent an average of the fuel gas composition between January and April of 2021. Propane concentration also takes into account C_{4+} since their concentrations are almost negligible compared to the other components, and it simplifies the following calculations.

Considering a 88% efficiency in the AC/DC converter, to obtain 1.06 MW of AC power, 1.2 MW should be produced by the fuel cell. It was also assumed a voltage of 0.8 V, and the current intensity was determined according to the following equation:

$$P = V \times I \tag{4.1}$$

Knowing that to generate 1kA, 0.038 kg H_2/ hr calculated in [112] for 1 505 kA, 56.7 kg/h is demanded. This was determined assuming that the fuel cells were arranged in parallel.

The utilization of fuel in a fuel cell is defined as the hydrogen consumed in the fuel cell ($H_{2,consumed}$)

by the total flow of hydrogen that enters the fuel cell ($H_{2,in}$):

$$U_f = \frac{H_{2,consumed}}{H_{2,in}} \tag{4.2}$$

To obtain an overproduction of hydrogen, U_f must be a reasonable value that fulfills hydrogen requirements for this CHHP system and still addresses a reasonable performance by the SOFC. Therefore, considering U_f of 85%, the hydrogen flow rate required to generate the desired DC power can be calculated as:

$$H_{2,in} = \frac{H_{2,consumed}}{U_f} = \frac{28.1}{0.85} = 33.0\frac{kmol}{h} = 56.7\frac{kg}{h} \tag{4.3}$$

Since this case study is not dealing with pure hydrogen but a mixture of hydrocarbons, to determine the fuel gas flow rate, stoichiometry of the possible reactions (1.3, 4.4, 4.5, 4.6) happening inside the fuel cell were taken into consideration. Reactions 4.4 to 4.6 combine the steam reforming and water-gas shift reactions for each hydrocarbon.

$$CH_4 + 2H_2O \leftrightarrow CO_2 + 4H_2 \tag{4.4}$$

$$C_2H_6 + 4H_2O \leftrightarrow 2CO_2 + 7H_2 \tag{4.5}$$

$$C_3H_8 + 6H_2O \leftrightarrow 3CO_2 + 10H_2 \tag{4.6}$$

Thus, by knowing the stoichiometry, fuel gas composition and, the amount of hydrogen available to react in the SOFC, the following relation can be establish to calculate fuel gas flow rate:

$$33.0 = n_{\text{fuel gas}} \times (0.408 + 0.334 \times 4 + 0.128 \times 7 + 0.130 \times 10) \Leftrightarrow n_{\text{fuel gas}} = 8.38\frac{kmol}{h} \tag{4.7}$$

Finally, to establish the air requirement, it is essential to observe that the stoichiometric ratio of hydrogen to oxygen is 2 to 1 for H_2O. Thus, the moles of oxygen required for the fuel cell reaction are half the hydrogen moles consumed by the fuel cell. An oxygen excess is performed in order to maintain the temperature profile inside the fuel cell, which was assumed to be three times higher than stoichiometrically needed to react with the amount of H_2 consumed. Because dry air contains 21% O_2 by volume or by mole, the required mass flow rate of dry air is 222.7 kmol/h.

4.3 Process Description

As mentioned before, the CHHP system was simulated using Aspen Plus V11 software. Fuel gas and air react in a SOFC where electrical energy and heat are produced. The anode outlet stream is employed for heat integration, and owing to its considerable amount of H_2, the possibility of recovering this component with high purity (+99.99%) is investigated. The flowsheet that represents the simulation discussed is presented in Appendix A, Fig.A.1. In order to simplify the explanation related to the development of this system, the process will be divided into two sections: heat and electricity production and hydrogen production.

4.3.1 SOFC process for Heat and Electricity production

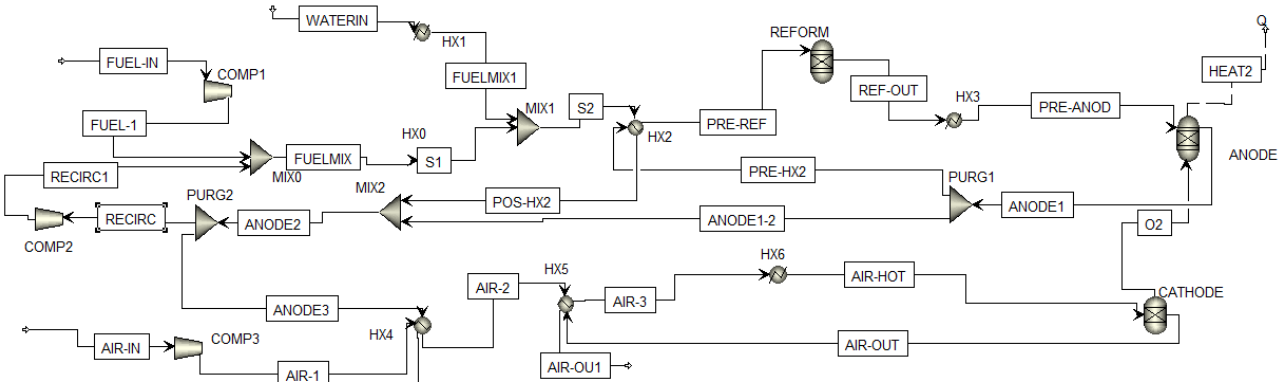

Figure 4.1: Flowsheet CHHP Simulation: Heat and Electrical Energy production.

Pre-Reforming

Fuel gas enters the CHHP system at atmospheric pressure suffering a slight increase by ”COMP1”. Part of the anode exhaust is recycled ”RECIRC1” (33%) to help to reach an H_2O-to-CH_4 ratio of 2.5–3.0, which is of standard practice in industry [113]. Nevertheless, fresh water, WATERIN, is also required to maintain this ratio. The feedstock is cleaned of contaminants that could degrade the system, such as sulfur (from the fuel) and salts (from the water). The cleanup subsystems were not modeled in Aspen since multiple technologies could be used, and many of them do not affect the mass and energy balance of the system significantly. The resulting mixture will be submitted to a partial reforming (block ”REFORM”) which limits the temperature gradient in the fuel cell from the endothermic reforming of light hydrocarbons and the exothermic electrochemical reactions. The chosen reactor was RStoic, operating at 700ºC. This reactor simulates precisely the reforming reactions specified below, and it considers as

input the intention of converting 20% of the existing hydrocarbons [113].

$$CH_4 + H_2O \leftrightarrow 3H_2 + CO \tag{4.8}$$

$$C_2H_6 + 2H_2O \leftrightarrow 5H_2 + 2CO \tag{4.9}$$

$$C_3H_8 + 3H_2O \leftrightarrow 7H_2 + 3CO \tag{4.10}$$

Anode

Before entering the anode compartment, the resulting gas (REF-OUT) passes through an electric heat exchanger, HX3, to increase the temperature to 850ºC, which corresponds to the working temperature of the SOFC chosen in this study [107]. In the ANODE block, the remaining hydrocarbons are reformed, CO is shifted. Stream "O2" delivers pure O_2 for H_2 oxidation. Ions transfer can not be modeled in Aspen Plus, therefore instead of the cell half-reactions, overall reactions 4.8 to 4.12 were simulated in this block model [114].

$$H_2 + 1/2O_2 \leftrightarrow H_2O \tag{4.11}$$

$$CO + H_2O \leftrightarrow CO_2 + H_2 \tag{4.12}$$

The "ANODE" block is characterized by the equilibrium reactor module RGibbs working in isothermal conditions. It reaches a rigorous reaction and/or multiphase equilibrium based on the Gibbs free energy minimization [115]. The anode outlet stream "ANODE1" is utilized for heat integration before being submitted to the hydrogen recovery process. It should be mentioned that the electrons flow, responsible for the DC current production, is also not possible to establish in Aspen Plus, thus semi-empirical equations (see Chapter 5, equations 5.1 to 5.5) were considered to determine the amount of electrical energy produced.

Cathode

Simultaneously, atmospheric air is submitted to a slight increase in pressure. Then, the intake air should reach the desired temperature, 850ºC, to carry out the electrochemical process in the fuel cell. This is performed by "HX4", "HX5" and "HX6", where in "HX4" and "HX5" heat integration is applied while "HX6"

corresponds to an electrical heat exchanger. Preheated air enters the cathode, modeled as a separator block (”CATHODE”) which simulates the mass transfer of oxygen ions required for the electrochemical reaction 4.11 [111]. Using this model, the amount of oxygen that is separated from the air and reacts with H_2 can be defined based on split fraction. This parameter was considered to be 0.3 since in section 4.2, it was assumed that the O_2 provided to the fuel cell was three times than the required to react with H_2.

Heat Integration

Reactions in block ”REFORMER” are endothermic. Thus part of the anode exhaust gas (”PRE-HX2”) is used to preheat the steam and fuel mixture up to a reasonable temperature for the catalytic reactor in block ”HX2”. Afterward, the remaining gas mixture that was not recycled back to the system, stream ”ANODE3”, serves as a hot utility in block ”HX4” for the air preheating process. Finally, the outlet stream depleted from O_2 (”AIR-OUT”) is also used for heat integration owing to its elevated temperature. It is responsible for the heat transfer in block ”HX5”. All the heat exchangers here mentioned are designed to have a 10 ºC minimum temperature approach [105].

4.3.2 Hydrogen Production

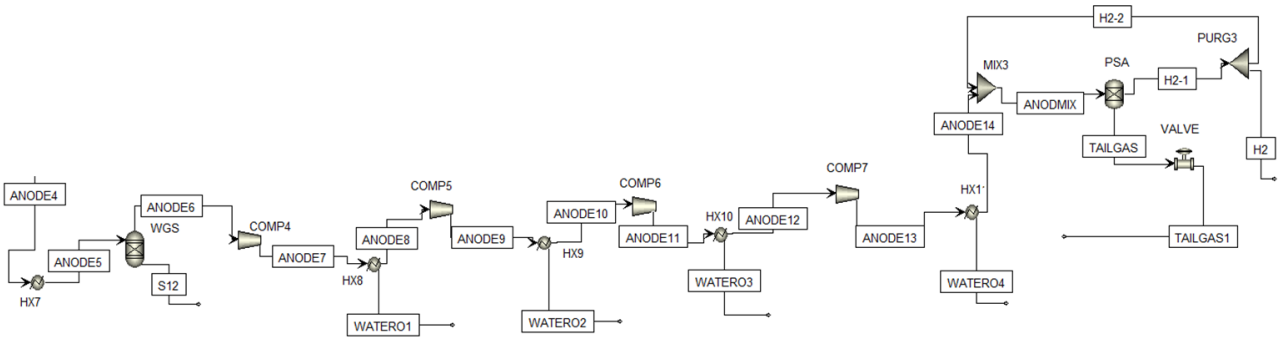

Figure 4.2: Flowsheet CHHP Simulation: Hydrogen production.

Water Gas Shift (WGS)

After being used for heat integration, stream ”ANODE 4” goes through a shift reaction and is diverted for purification and storage of hydrogen. Therefore, it is cooled down to 300 ºC, which is favorable for the WGS reaction. The anode tail-gas stream in the presence of a WGS catalyst is assumed to be in shift equilibrium in the model where reaction 4.13 takes place [40]. REquil (”WGS”) was the block chosen to

simulate this reaction considering ”Temperature Approach” as specification type.

$$H_2O + CO \leftrightarrow CO_2 + H_2 \tag{4.13}$$

Pressure Swing Adsorption

The optimum feed pressure to the PSA ranges from 15 to 29 bar [5]; the inlet pressure for this model is chosen to be 18 bar. A multi-stage compressor represented by ”COMP4” to ”COMP7” is used with a maximum compression ratio of 2:1 per stage and intercoolers to 25℃. In the Aspen model, water is removed after each compression stage [113]. The PSA unit is modeled as a separator block. The composition requirement for hydrogen at the inlet of the PSA unit is 70% or higher for the process to be economical and reach 85% hydrogen separation with adequate purity (99.99+%) [40]. Therefore, the split fraction considered in ”PSA” was 0.85 for hydrogen. To achieve 70% content of this component in the feed gas, 88 % of the purified hydrogen is recycled to the PSA inlet, represented by the stream ”H2-2”. This modeling approach is consistent with other work in the literature [116], and it is adequate for high-level performance estimation of the PSA unit. The ”TAILGAS” stream will be depressurized and used for heating applications.

Chapter 5

Results and Discussion

5.1 SOFC Modelling

SOFC modeling has as main objective to generate the expected stack performance and express its sensitivity to temperature, pressure, and compositional variations in the reactant feed gases. Aspen Plus software does not allow determining the cell's voltage and, consequently, power production, which are crucial parameters to validate the implemented system and preliminary calculations. Two different approaches were used to determine the cell voltage. Note that due to the lack of detailed information on the SOFC, values of specific parameters are from the literature.

5.1.1 Approach 1

The method used in the proposed model combines a performance curve obtained by interpolation of experimental data at standard operating conditions, as a reference. Afterward, it predicts the cell voltage by applying semi-empirical correlations [112, 117]. These equations account for the effects of operating pressure, temperature, current density, and fuel/ air composition on the actual voltage. In this way, cell performance can be predicted using Aspen Plus V11 data and applying the following equations in the Excel tool. The current model adopts an experimental curve published in the Fuel Cell Handbook [112] as the reference curve to define the reference voltage V_{ref} at the referenced operating condition (inlet fuel composition: 67% H_2, 22% CO, 11% H_2O, 85% U_f, T=1000 ºC and P=1 bar). Regarding the semi-empirical equations, they are [112, 117]:

- Operating pressure:

$$\Delta V_{\mathrm{p}}(mV) = 76 \times log\frac{P}{P_{\mathrm{ref}}} \tag{5.1}$$

where P is the operating pressure (bar) and P_{ref} is the reference operating pressure (here P_{ref}=1 bar).

- Operating temperature and current density:

$$\Delta V_{T}(mV) = 0.008 \times (T - T_{ref})(C) \times I_{c}(mA/cm^{2}) \tag{5.2}$$

where T is the operating temperature and T_{ref} is the reference operating temperature (here T_{ref}=1000 ºC). The current density defined as I_c was considered 80 A/cm^2 (see Figure 5 in [118]).

- Fuel composition:

$$\Delta V_{anode}(mV) = 172 \times log \frac{P_{H_2}/P_{H_2O}}{(P_{H_2}/P_{H_2O})_{ref}} \tag{5.3}$$

where P_{H_2}/P_{H_2O} is the ratio of H_2 and steam partial pressures in the system and $(P_{H_2}/P_{H_2O})_{ref}$ is the ratio of H_2 and steam partial pressures in the system under reference conditions (here $(P_{H_2}/P_{H_2O})_{ref}$=0.15).

- Oxidant composition:

$$\Delta V_{cathode}(mV) = 92 \times log \frac{P_{O_2}}{(P_{O_2})_{ref}} \tag{5.4}$$

where P_{O_2} and $(P_{O_2})_{ref}$ are the average oxygen partial pressures at the cathode for the actual case and the reference case, respectively ($(P_{O_2})_{ref}$=0.164).

Note that in the ΔV_{anode} and $\Delta V_{cathode}$, the values of P_{H_2}, P_{H_2O} and P_{O_2} correspond to an average between the inlet and outlet of the fuel cell [119]. By summing the four correlations, the actual voltage V can be calculated as:

$$V = V_{ref} + \Delta V_{T} + \Delta V_{P} + \Delta V_{anode} + \Delta V_{cathode} \tag{5.5}$$

The fuel cell power output is the product of the cell voltage and current. The developed model takes the desired power output as an input to calculate the corresponding voltage and current required to generate the power. Then, if the product between these parameters does not match the desired power output, the amount of fresh fuel is corrected according to the hierarchy of the calculations is shown in Fig. 5.1.

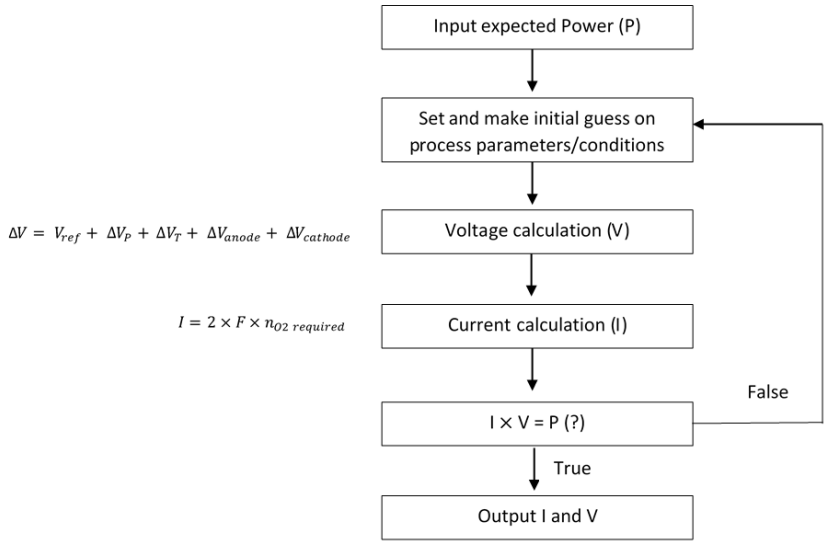

Figure 5.1: Order of cell voltage calculations.

5.1.2 Approach 2

On this approach, the cell voltage is determined through equation 5.6 [105]. Herein, the fuel cell operating conditions were also modeled based on the inlet and outlet's average temperature and fuel composition. The nominal operating temperature of the stack is estimated to be 850 ºC with a per-pass fuel utilization of 85%.

$$V = OCV_{\text{Nernst}} - \eta_{\text{act}} - \eta_{\text{ohm}} - \eta_{\text{conc}} \tag{5.6}$$

where OCV_{Nernst} is the open circuit voltage, and the η terms are the activation, ohmic, and concentration losses described below. The OCV_{Nernst} accounts for temperature and composition dependence of the Nernst voltage, as well as the deviation of the experimental OCV voltage from theory in agreement with:

$$OCV_{\text{exp}} = E_0 + \frac{RT}{nF} ln\Big[\frac{P_{\text{H}_2} {P_{\text{O}_2}}^{0.5}}{P_{\text{H}_2}O} {P_{\text{atm}}}^{0.5}\Big] \tag{5.7}$$

where from [117]

$$E_0 = 1.2723 - 2.7645 \times 10^{-4} \times T \tag{5.8}$$

and n = 2 and F = 96 485 C mol^{-1}. Deviation of the experimental OCV from the Nernst voltage is accounted in:

$$\theta = \frac{OCV_{\text{exp}}}{OCV_{\text{Nernst}}} \tag{5.9}$$

where θ refers to the electronic and ionic conductivity of the electrolyte in open circuit conditions [120]. This factor is approximately 0.94 [120]. The activation polarization, η_{act}, is inherently calculated from the

Butler–Volmer equation:

$$j = j_0\Big[exp\Big(\alpha\frac{nF}{RT}\eta_{\text{act}}\Big) - exp\Big(-(1-\alpha)\frac{nF}{RT}\eta_{\text{act}}\Big)\Big] \tag{5.10}$$

where α is the charge transfer coefficient, and j_0 corresponds to a pre-exponential factor specific to each electrode expressed by:

$$j_{0,\text{c}} = \gamma_{\text{c}}\Big(\frac{P_{O_2}}{P_{\text{atm}}}\Big)^{0.25}exp\Big(-\frac{E_{\text{act,c}}}{RT}\Big) \tag{5.11}$$

$$j_{0,\text{a}} = \gamma_{\text{a}}\Big(\frac{P_{H_2}}{P_{\text{atm}}}\Big)\Big(\frac{P_{H_2O}}{P_{\text{atm}}}\Big)exp\Big(-\frac{E_{\text{act,a}}}{RT}\Big) \tag{5.12}$$

where γ is an activation over-potential factor and E_{act} is the activation energy; these values are obtained from [121] and are presented in Table 5.1. The charge transfer coefficient, α, typically ranges from 0.2 to 0.5 [122]. Furthermore, in reversible reactions (an usual assumption made for SOFC kinetic behaviour), the chemical and electrical energy form equal activation barriers for the forward and reverse reactions, thus α= 0.5 [122]. This simplification is used to reduce the B–V equation 5.10 to:

$$j = 2j_0 sinh\Big(\frac{nF}{2RT}\eta_{\text{act}}\Big) \tag{5.13}$$

The ohmic loss term, η_{ohm}, is dependent on both the resistivity of the stack components, and their thicknesses. An area specific resistance may be employed as an approximation for this dependence:

$$\eta_{\text{ohm}} = j \times ASR_{\text{ohm}} \tag{5.14}$$

where ASR_{ohm} is the ohmic area specific resistance estimated from [121] to be 0.04 Ω cm^2. The concentration losses, η_{conc}, are obtained by the limiting current density in the subsequent equation:

$$\eta_{\text{conc}} = \frac{RT}{nF}ln\Big(1 - \frac{j}{j_{\text{L}}}\Big) \tag{5.15}$$

where j_{L} is the limiting current density and is predicted to be 1.6 A/cm^2 at 800 ºC from [123].

Although the method employed to determine the cell voltage is completely distinct from the one presented in **subsection 5.1.1** the hierarchy of calculations also follows the one presented in Fig. 5.1.

The following table gathers the parameters stated throughout the text and that are used as input.

Table 5.1: Model parameters [105].

R	8.31	J mol^{-1}
T	1123	K
n	2.00	-
F	96 485	C mol^{-1}
γ_{an}	5.50E+12	A cm^{-2}
γ_{cat}	7.00E+12	A cm^{-2}
$E_{act,\ a}$	1.00E+05	J mol^{-1}
$E_{act,\ c}$	1.20E+05	J mol^{-1}
α	0.500	-
ASR_{ohm}	0.040	Ω cm^{2}
j_L	1.600	A cm^{-2}
j	0.080	A cm^{-2}

5.1.3 Results

Table 5.2 presents the results obtained using the input data determined in **section 4.2** and applying both approaches to calculate the cell voltage, consequently confirming whether the power output corresponds to the one desired or not. All calculations performed for the following data can be found in **Appendix B**, tables B.1 to B.3.

Table 5.2: Results of SOFC Modelling for the CHHP system developed in Aspen Plus V11.

	Approach 1	Approach 2	Units
n_{fuel}	8.38		kmol h^{-1}
n_{air}	222.7		kmol h^{-1}
$n_{fresh\ water}$	4.7		kmol h^{-1}
I	1 504		kA
ΔV	0.873	0.812	V
P_{DC}	1.312	1.221	MW
P_{AC}	1.155	1.075	MW

Results indicate that Approach 2 determines a cell voltage quite accurately with the one considered by Bloom Energy (0.8 V). Thus, the output power (AC) obtained by this method presents only a relative error of 14% for the desired power, which suggests that the calculations performed in advance to test the model were an acceptable approximation. Contrarily, Approach 1 presents a higher cell voltage and, therefore, a higher output power (AC), with a relative error of 90%. Nevertheless, both results show that the output power (AC) is higher than expected, meaning that the amount of current produced is exceeded. Therefore, the fuel and, ergo, oxidant flow reacting in the SOFC should be lowered.

As explained before, the fuel flow and, consequently, oxidant flow were adjusted until the desired power output was reached. It should be mentioned that for every attempt, the water flow is also correct in order to respect the S/C ratio.

Table 5.3 presents the input data for the desired power. One can note that the cell voltage is equal in both approaches, even though the amount of hydrogen consumed changed. Nevertheless, this differ-

Table 5.3: Final Results of SOFC Modelling for the CHHP system developed in Aspen Plus V11.

	Approach 1	Approach 2	Units
n_{fuel}	8.27		kmol h^{-1}
n_{air}	219.8		kmol h^{-1}
$n_{fresh\ water}$	4.6		kmol h^{-1}
I	1 485		kA
ΔV	0.873	0.812	V
P_{DC}	1.296	1.206	MW
P_{AC}	1.140	1.060	MW

ence does not even correspond to 1 kmol/h, meaning that these models may not be sensitive enough to influence the outcome voltage, although it changes the current intensity since it is directly proportional to the amount of hydrogen consumed. Sensitive analysis will be further performed in order to evaluate this issue in more detail.

Both approaches show a decrease in the output power (AC), yet, in Approach 2, the value obtained for this parameter corresponds exactly to the one desired while in Approach 1 it is higher. It is possible to conclude that Approach 2 is more accurate than Approach 1, which was already expected since it takes into account activation, ohmic polarization, and concentration losses with a temperate and pressure dependency (see equations 5.13, 5.14, 5.14). Additionally, it is the SOFC model generally used in the research community. Whilst Approach 1, even though it is a reliable method to apply, considers semi-empirical equations that account only for the effects of operating pressure and temperature, current density, and fuel/air composition on the actual voltage. However, the voltage losses in SOFCs are governed by ohmic losses in the cell components, which are not directly accounted on this Approach and may be a valid reason for the difference observed [112]. Thus, in the following subjects, Approach 2 was the one considered to determine the SOFC parameters.

5.2 Hydrogen and Heat Production

Hydrogen and heat production are also crucial parameters to be examined in this study. Using the results obtained in Table 5.3 and implementing the specifications stated in **subsubsection 4.3.2**, H_2 flow is 3.9 kg h^{-1} corresponding to a daily production of 95 kg day $^{-1}$ (31.4 ton $year^{-1}$).

Regarding the heat produced, stream TAILGAS1, with an enthalpy of 3.02 MMBtu h^{-1}, could be used for a building heating system or a water cycle, entering at 60℃ and being heated up to 80℃ before returning to the facility. Nevertheless, this part was not simulated in Aspen Plus in order to simplify the system developed and since the amount of heat produced is almost negligible.

There is an additional interest in hydrogen over-production and considering that the value obtained is

quite inferior in comparison to the three methods for hydrogen production presented in Table 5.4, U_f was decreased by maintaining the same amount of oxidant entering the cathode but increasing the amount of fuel entering the anode.

Table 5.4: Comparison between the amount of hydrogen produced from different processes [105].

Process	H_2 Production	Units
SMR of Natural Gas (large-scale)	150 000	kg day^{-1}
SMR of Natural Gas (distributed-scale)	250	kg day^{-1}
Electrolysis	1 050	kg day^{-1}

Table 5.5: Results for hydrogen over-production in CHHP implemented on Aspen Plus.

Parameter	Value	Units
n_{fuel}	10	kmol h^{-1}
n_{air}	219.8	kmol h^{-1}
$n_{fresh\ water}$	6.50	kmol h^{-1}
ΔV	0.817	V
I	1 485	kA
P_{DC}	1.213	MW
P_{AC}	1.067	MW
H_2 production	16.5	kg h^{-1}
H_2 production	396	kg day^{-1}
H_2 production	130 680	kg $year^{-1}$

Results demonstrate a considerable increase in hydrogen production with the change from 8.27 kmol h^{-1} to 10 kmol h^{-1} of fuel. An impact on the cell voltage is also observed. The SOFC operating voltage increases slightly (5 mV) due to a higher content of reactant hydrogen (which increases the Nernst potential) and a reduction in U_f. Nevertheless, as it was expected, the power output remains approximately equal (mass balances related to this scenario for the main equipment in the system are in Appendix B, Table B.4 to Table B.8). The desired value of hydrogen production will only be possible to examine with the Economic Analysis of the system implemented. Once again, fuel and oxidant flow will be further corrected.

5.3 Validation of the Simulation Results

To validate not only the methods applied for the voltage cell calculation but the overall CHHP system established in Aspen Plus, this system will be submitted to the conditions of two different studies from the literature: Case Study 1 ([40]) and Case Study 2 ([105]). The goal is to compare the results obtained with the ones provided by these studies and conclude on the feasibility of the CHHP system implemented. Moreover, concerning only the SOFC, Bloom Energy has data available for a 100kW system which was also tested [124].

5.3.1 100 kW Bloom Energy Server

The Bloom Energy's 100 kW unit consumes 0.661 MMBtu hr^{-1} of natural gas, which corresponds to a 14.37 kg hr^{-1} flow. This system operates at 950ºC [124]. Since no more information was provided, it was assumed that air enters the cathode with O_2 in excess (around three times to the amount needed to react), there is a pre-reforming of the natural gas before reaching the anode, and fresh water is added to maintain the S/C ratio. Only the SOFC was evaluated since there is no further information regarding a possible hydrogen or heat production.

Table 5.6: Results for Bloom Energy 100kW Server.

Parameters	Value	Units
n_{fuel}	0.763	kmol hr^{-1}
n_{air}	24.2	kmol hr^{-1}
$n_{fresh\ water}$	2.07	kmol hr^{-1}
I	164	kA
ΔV	0.781	V
P_{DC}	128	kW
P_{AC}	109	kW

The results indicate that there is a discrepancy of 9% between the value obtained by the implemented system and the one according to Bloom Energy. Since there is a scarce amount of information regarding this SOFC Server to implement it in Aspen Plus and, as said, above there were several assumptions performed. Nevertheless, the results are closed enough to conclude that the SOFC developed is a reasonable approximation to the one designed by Bloom Energy.

5.3.2 Case Study 1

SOFC Simulation

The developed model was validated with published data for the analysis of a 1 MW SOFC polygeneration system for combined production of heat, hydrogen, and power, operating on methane [105]. The model inputs were as follows:

- Methane and air inlet flow: 0.039 and 1.849 kg s^{-1}, respectively;
- Methane and Air compressed to 20kPa above atmospheric pressure to account for pressure loss of the system;
- S/C ratio: 2.9;
- Anode exhaust gas recycle of 65%;
- Cold and hot stream temperature difference: 10 ºC;

- Air stoichiometric factor: 3.3;
- Pre-reforming 20% of the CH_4 in the fuel mixture;
- Operating temperature of pre-SMR: 700ºC
- SOFC operating temperature: 725ºC;
- DC to AC inverter efficiency: 83%.

Table 5.7: Results for Case Study 1.

Parameters	Value	Units
n_{fuel}	8.76	kmol hr^{-1}
n_{air}	230.7	kmol hr^{-1}
$n_{fresh\ water}$	0.400	kmol hr^{-1}
I	1549	kA
ΔV	0.832	V
P_{DC}	1.29	MW
P_{AC}	1.07	MW

The case study under evaluation mentions that the SOFC gross power MWe AC was 1.14 while the system implemented considers an output power of 1.07 MW. Thus, the model results are in good agreement with published work. It should be pointed out that there isn't any comment on the use of fresh water. However, in order to respect the S/C ratio, it was considered.

Hydrogen Production

Concerning the input parameters for hydrogen production, they are:

- Operating temperature for WGS reaction: 300ºC;
- Operating temperature for PSA: 40ºC;
- Operating pressure for PSA: 18 bar;
- Compression ratio 2:1;
- Tail gas with 70% molar composition in H_2 entering PSA;
- Separation in PSA: 85%:

The simulation calculates that an amount of 131.8 kg day^{-1} of H_2 with (+99,999%) is produced. This value is in agreement with the one provided in [105]. Furthermore, it was also analyzed hydrogen over-production. The requirement was to produce an extra 100 kg H_2 day^{-1} from the baseline case. This requirement was accomplished by feeding excess methane (0.042 kg s^{-1}) into the system, while the

electric power requirement is still 1 MW AC. All the component sizes, including the SOFC, remain the same.

Table 5.8: Results for Case Study 1, with hydrogen over-production.

Parameters	Value	Units
I	1549	kA
ΔV	0.856	V
P_{DC}	1.33	MW
P_{AC}	1.10	MW
H_2 production	232	kg day^{-1}
H_2 production	76 428	kg $year^{-1}$

It is possible to observe that there is an increase in the cell voltage, around 20 mV, which was expectable due to a higher content of hydrogen reactant. The daily hydrogen production increased an extra 100 kg hr^{-1} as it was desired, and it is in agreement with the value estimated in the literature (238 kg H_2 hr^{-1}). Additionally, the intention of increasing the amount of hydrogen produced makes it comparable to the hydrogen production on SMR of Natural-Gas on a distributed scale.

5.3.3 Case Study 2

This case study evaluates the implementation of 1 MW SOFC CHHP system operated on methane using Aspen Plus simulation software [113]. Both SOFC simulation and hydrogen production will be analyzed together since, in this case, there isn't any requirement to further change the input data. The model input data provided is:

SOFC Simulation

- Methane and air inlet flow: 8.18 and 177.5 kmol h^{-1}, respectively;
- Methane and air inlet temperature: 20ºC;
- Methane and air inlet pressure: 1.38 bar;
- S/C ratio: 2.5 to 3;
- Anode exhaust recycle of 65%;
- Air stoichiometric factor: 3.2;
- Pre-reforming 20% of the CH_4 in the fuel mixture;
- Operating temperature of pre-SMR: 700ºC;
- SOFC operating temperature: 800ºC;

- DC to AC inverter efficiency: 88%;

Hydrogen Production

- Operating temperature for WGS reaction: 300ºC;
- Operating temperature for PSA: 30ºC;
- Operating pressure for PSA: 10.4 bar;
- Compression ratio 2:1;
- Separation in PSA: 85%:

Table 5.9: Results for Case Study 2.

Parameters	Value	Units
n_{fuel}	8.175	kmol hr^{-1}
n_{air}	177.5	kmol hr^{-1}
$n_{fresh\ water}$	0,4	kmol hr^{-1}
I	1458	kA
ΔV	0.829	V
P_{DC}	1.21	MW
P_{AC}	1.06	MW
H_2 production	225.8	kg day^{-1}
H_2 production	74 527	kg $year^{-1}$

Firstly, the output power produced indicates that the defined system is in accordance with the one provided by the case study. The hydrogen production considered in the literature is 229.2 kg day^{-1} in contrast with the value obtained by the model results, which indicate a daily production of 225.8 kg.

To conclude, it is possible to affirm that the system implemented in Aspen Plus and the SOFC model chosen to determine the cell voltage present accurate results. Therefore, one of the main purposes of this work, develop a computer simulation model flexible enough to be applied in industry and capable of predicting a valid system performance under different operating conditions and using various fuels, was accomplished.

5.4 Sensitivity Analysis

Aspen Plus software provides the possibility to perform sensitivity analysis, which simplifies understanding the effects of variations of the operating parameters on the SOFC's performance. The following section exhibits the results of several sensitivity analyses executed using Aspen Plus. All assumptions referred in **Chapter 4** are kept the same.

The utilization factor is one of the most important operating parameters for fuel cells and has significant effects on the cell voltage and current intensity [112]. Figures 6.1 and 6.2 depict the influence of U_f on SOFC stack performance, for both cell voltage and current intensity.

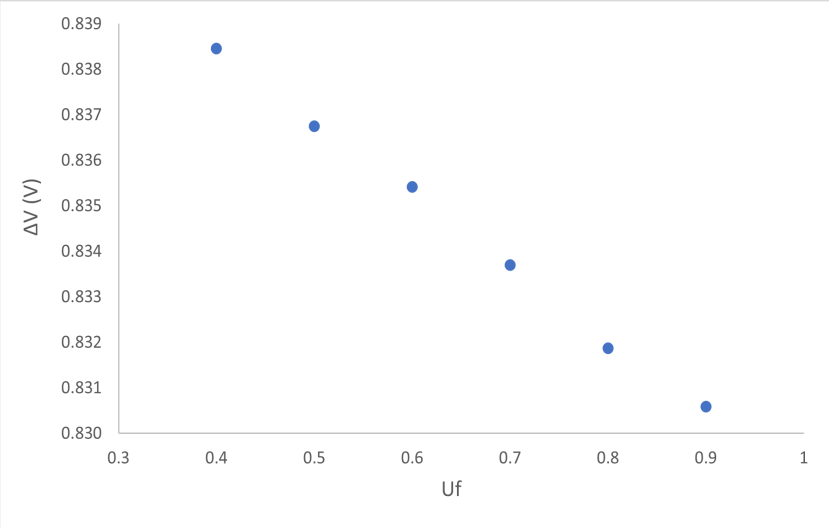

Figure 5.2: Effects of U_f on the cell voltage.

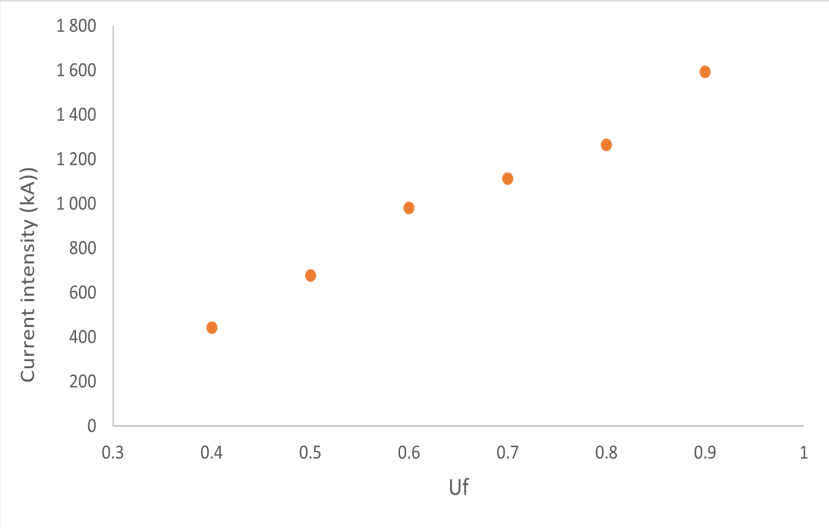

Figure 5.3: Effects of U_f on the current.

Increasing U_f from 0.4 to 0.9, implies a decrease in the cell voltage since the fuel is more depleted and the voltage losses at the anode are increased. In contrast, the current intensity will increase, which can be accomplished by increasing the airflow, resulting in more H_2 being consumed in the anode (I = $2FnH_2$,consumed) [117, 125]. Therefore, operating the SOFC stack at high fuel utilization promotes a higher current intensity and, consequently, higher power output. However, it should be analyzed if the voltage losses aren't increasing substantially. Usually, 0.85 for the U_f is considered [119, 125].

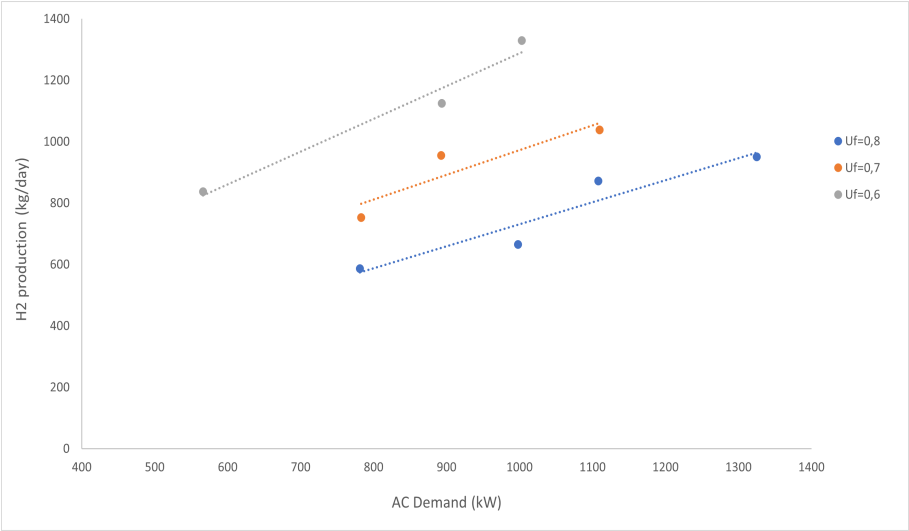

Figure 5.4: Effects of AC demand on the Hydrogen Production.

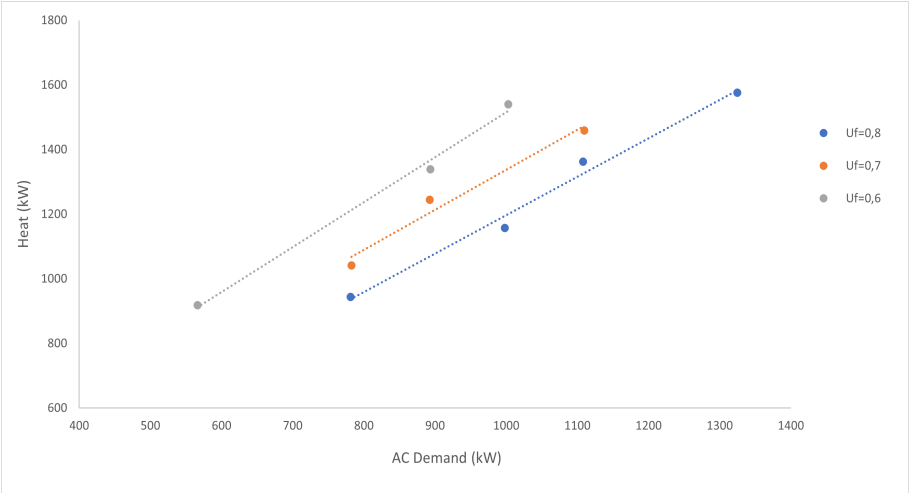

Figure 5.5: Effects of AC Demand on the Heat Production.

Besides evaluating the SOFC performance for power production, since this system also aims to produce other forms of energy, heat, and hydrogen, these were also submitted to sensitive analysis at different values of U_f.

It is possible to observe that for each value of U_f both hydrogen and heat production increase with the increase in AC power output demand.

Regarding hydrogen production, a higher amount of fuel gas input is reformed and, with a constant U_f, the hydrogen not consumed by the fuel cell increases in the same proportion that hydrogen is converted in the electrochemical reaction. Moreover, decreasing the U_f leads to an increase in hydrogen production, which was already expected since less hydrogen is consumed by the SOFC, being available for the recovery process. Lastly, values between 600 and 1 200 kg day^{-1} are possible to reach, which is comparable to the amounts claimed to be produced in table 5.4, therefore justifying the possible

feasibility of this project.

The heat produced will increase with the increase in AC demand because this corresponds to an increase in the amount of products formed, and this electrochemical reaction is exothermic. Increasing U_f translates in more H_2 converted to electricity, meaning less is available to the combustion plenum, thus lowering the combustion temperature and, in consequence, the cathode and stack exhaust temperatures, as well as the amount of heat produced [119].

Chapter 6

Economic Analysis

An economic analysis of the studied system is crucial to determine whether it is worth the investment carried out. Thus, it was considered a 3 years duration for the project investment and construction and 20 years for the exploration period.

According to [126] SOFCs should be replaced every five years. In order to have more detailed information in what concerns maintenance services, an attempt to contact Bloom Energy was made. However, no response was received and thus it was assumed the worst case scenario which considers an acquisition of new servers every five years [126].

The total investment of this CHHP system was determined, as well as operation costs. Lastly, taking these into account and the generated profit regarding electrical energy and hydrogen production, it was possible to evaluate the economic benefits of the project. The payback time (time the project takes to recover the invested capital) is also determined [127].

6.1 Total Investment

The total investment is divided in three parts: fixed capital, circulating capital, and interim interest. The fixed capital is related to all the costs concerning the installation of the system. Whereas circulating capital corresponds to the capital consumed in the process of production. Interim interests are associated with project financing [128]. This project will only focus on determining the fixed capital investment since to calculate the circulating capital and interim interest with a certain accuracy, a detailed engineering project ought to be performed.

Fixed capital is divided into two main groups: direct costs and indirect costs [128]. Regarding direct costs, these include equipment base costs which will be analyzed in further detail.

Equipment costs were estimated using the cost scaling equation given in equation 6.1. The cost of each scaling unit (S) is established using the reference scaling unit (S_0) and its base cost (C_0). The superscript *n* corresponds to the scaling factor, which considers the economy of scale of a particular component. Using the Chemical Engineering Plant Cost Index (CEPCI), the cost is updated following the changes in the value of money due to inflation and deflation. The installed cost (IC) is then determined by using an installation factor (I_F), which takes into account the multiple costs associated with installing each equipment [105].

$$IC = \Big(\frac{S}{S_0}\Big)^n \Big(\frac{CEPCI}{CEPC_0}\Big) I_F \tag{6.1}$$

Table C.1 in Appendix C presents the component cost breakdown of the plant related with the results presented in Table 5.5. Reference costs are calculated from either scaling literature data or using an online equipment cost estimator or via the economic analyzer within ASPEN Plus as explained in the table footnotes. The SOFC costs were calculated considering the price provided by Bloom Energy of 4 000 $/kW [109].

The equipment and installation costs are included in the direct costs (DC). These also consider utilities, services, piping, instrumentation, control, buildings, electrical installation, and thermal isolation costs. To estimate these, a percentage on the equipment base cost was considered, as demonstrated in Table 6.1 [128].

Table 6.1: Direct costs for the CHHP system.

	Cost (M€)	Factor (%BE)
Base Equiment (BE)	5.808	-
Piping	1.452	0.25
Services and Utilities	0.580	0.10
Control and Instrumentation	0.290	0.05
Buildings	0.290	0.05
Electrical Installations	0.580	0.10
Thermal Insulations	0.464	0.08
Total	9.47	

In addition to direct costs, the indirect costs shown in Table 6.2 include engineering and design, plant construction, legal and contractors fees, and project contingencies. They are also determined following the same scheme used for direct costs. Nevertheless, each element accounts for a percentage of direct costs and not equipment base cost [128].

In this manner, the total investment respecting the CHHP system established is 13.54 M€. This value is higher than the one determined in [105] which is approximately 4.66 M€. The main factor for this discrepancy is related to the SOFC system cost, which in [105] is 0.850 M€ in comparison with 4.001 M€ provided by Bloom Energy. Nevertheless, the referenced value in [105] is obtained through the literature based on the US Department of Energy cost target for SOFC systems and not in the actual

Table 6.2: Indirect costs for the CHHP system.

	Cost (M€)	Factor (% DC)
Engineering and Design	1.42	0.15
Site prep and construction	1.42	0.15
Project contingency[1]	1.23	0.10
Total	4.07	

value of these systems in the market [129]. Moreover, in [105] direct costs only account base equipment while herein other predictable costs were taken into consideration, which, consequently, increased the total investment.

6.2 Consumption Costs and Production Profit

The consumption costs taken into consideration were related to fuel gas, water, and electrical energy. However, it should be pointed out that the electrical energy consumption of the trigeneration system is self-supported.

Firstly, the electrical consumption of the equipment in the CHHP system was determined to understand the amount of electrical energy available to provide to the GTs auxiliary equipment in the Cogeneration facility at Sines' Refinery. This parameter was determined using the Aspen Plus V11 software tool. Only the heat exchangers that were not a part of the heat integration were considered. The electrical energy used in the start-up of the SOFC was not considered since it will be auto-supported throughout the operation. Considering that the PSA was simulated as a separator block in Aspen Plus, it was not possible to determine its electrical consumption. Thus it was not accounted for the overall consumption of this system. The consumption of the leading equipment is described in the table below.

Table 6.3: Electrical consumption of the main equipment in CHHP system.

Equipment	HX1	HX3	REFORM	HX6	Multi-stage COMP	Total
Electrical Consumption (kW)	100.1	73.7	70.2	123	95.6	463.5

It is possible to observe that this system has a considerable consumption of electrical energy. The amount of electrical energy available for the cogeneration system is only 603 kW, far inferior to the one expected to deliver. The calculations and tests performed in Chapters 4 and 5 didn't considered this feature. However, in order to fulfill the requirement of electrical energy available for the cogeneration system, different input conditions were applied.

Considering 15.23 mol h^{-1} of fuel, 10 kmol h^{-1} of water and 357.1 kmol h^{-1} of air the total of energy produced by the SOFC is 1.744 MW for a total investment of 20.045 M€ (see Appendix C, Table C.2

[1] Percentage based on the total of direct and indirect costs.

and Table C.3 for further information regarding SOFC modelling and CHHP total investment). Table 6.4 presents each equipment's auto-consumption and the total electrical energy required to sustain them.

Table 6.4: Electrical consumption of the main equipment in the 1.744 MW CHHP system.

Equipment	HX1	HX3	REFORM	HX6	Multi-stage COMP	Total
Electrical Consumption (kW)	155	113	107	200	140	715

With the new data, it is possible to determine that 1.03 MW of electrical energy is available for GTs auxiliary equipment. Even though, it doesn't correspond precisely to the intended electrical power output, it is the most reasonable scenario taking into account that a higher power output leads to an non-linear increase in equipment's auto-consumption. Table 6.5 presents the consumption and production associated with each component on an hourly and daily basis, which will be needed for further calculations.

Table 6.5: Consumption and Production of the main components in the 1.744 MW CHHP system.

Component	Consumption		Production	
	Hour	Day	Hour	Day
Fuel Gas (kWh)	3 607	86 560	-	-
Electrical Energy (kWh)	715	17 171	1 744	41 856
Hydrogen (kg h^{-1})	-	-	19.2	461
Water (kg h^{-1})	180	4 324	476	11 421
Heat (MMBtu)	-	-	5.53	133

Regarding the cost designed for each component (see Appendix C, Table C.4), most were provided by Galp. In the heat produced, the cost was determined as a fraction of the natural gas cost proportional to its calorific power. The cost of the hydrogen produced was slightly more challenging to establish. On average, the total capacity of a FCEV is around 5 kg of hydrogen [130]. Considering that hydrogen with a 99.999% purity costs between 10-20€ kg^{-1} and that full storage is worth 50-60€, in order to be competitive in the market, the price of 12€ kg^{-1} of hydrogen was settled [131, 132]. The water cost was not accounted, it is only presented to verify that the water produced in the system surpasses the required amount of freshwater. The excess will be supplied to the other facilities at Sines Refinery.

Lastly, the daily costs and possible profit regarding the trigeneration system throughout evaluation are expressed in Table 6.6. It shows that 1 653 € of fuel gas will be spent daily, to obtain savings in electricity imports in the order of 2 469 € and a profit on hydrogen and heat around 5 530 € and 580 €, respectively. With these values, a daily positive balance of 6 924€ is reached.

Table 6.6: Production vs consumption analysis of the 1.744 MW CHHP system.

Component	Fuel Gas	Electrical Energy	Hydrogen	Heat
Cost	0.0191	0.100	12.0	4.37
Hourly Availability	3 607	1 029	19.2	5.50
Daily Availability	86 560	24 685	461	133
Cost (€ day^{-1})	1 653	2 469	5 530	580

Before studying the profitability with the data provided along with this chapter, there is one crucial aspect that should also be analyzed in further detail, which is related to CO_2 emissions. These emissions remain the main factor in greenhouse gases, and their increase occurs mainly due to the harmful use of polluting (non-renewable) energies. Consequently, taxes on carbon emissions are imposed in most countries in order to mitigate pollutant emissions [133]. Nowadays, these have reached around 50 € ton^{-1} of CO_2 emitted. Nevertheless, this value is increasing substantially in the past months, and the tendency is to continue. Ideally, a SOFC only produces water if fuelled with pure hydrogen, since in this case, there are other components in the fuel, CO_2 will be produced. Yet, these emissions are still lower (0.308 kg/kWh) than the ones produced in a conventional electric power facility (0.429 kg kWh^{-1}) [134, 135]. Hence, the amount of capital saved using this system to produce electrical energy was considered a profit and will be included in the revenue obtained from the amount of electricity, hydrogen, and heat produced.

Table 6.7: CO_2 emissions and savings for the 1.744 MW CHHP system.

	SOFC	Power Plant	Units
CO_2 emissions	0.308	0.429	kg kWh^{-1}
Power	1 744		kWh
CO_2 emissions	0.538	0.748	ton/h
CO_2 emissions	4 297	5 979	ton $year^{-1}$
Carbon tax	50.0		€/ton
Total fare	214 831	298 971	€
Savings	84 140		€

6.3 Investment Performance Indicator - Payback

A performance indicator of an investment project corresponds to an index calculated from the financial flows of the project. It attempts to measure a specific dimension of the quality of the investment. One performance indicator is the Payback, defined as the time required for a project to recover the capital invested. It is considered a measure of project risk [130].

Table 6.8: Payback analysis of the 1.744 MW CHHP system.

Total Investment (M€)	20.05
Annual Consumption (M€)	0.551
Annual Production (M€)	2.941
Payback	8

Considering an investment of 20.05 M€, a return would be obtained after 8 years and 4 months, taking into account that this scenario is quite conservative since the hydrogen price is close to the reference minimum. As mentioned at the beginning of this chapter, the medium life expectancy of a SOFC stack is around 5 years. Since the worst case scenario (replacing the SOFC Servers) is considered, Payback should be below this value. Not only to recover the investment performed but also to generate considerable profit before purchasing this equipment that, as also seen, is the most expensive one.

Two tests were performed to understand which variable between the generated power and hydrogen produced influences the Payback. First, the U_f was reduced from 0.75 to 0.70 to acknowledge a higher amount of hydrogen produced for the same electrical energy delivered. Then, the desired AC output available was increased from 1037 kW to 1154 kW, maintaining the same U_f used in the results presented in Table 6.8, 0.75.

Table 6.9: Comparison of different scenarios for the 1.744 MW CHHP system regarding electrical energy and hydrogen production.

Scenario	1	2	3
Uf	0.75	0.70	0.75
Available Output Power AC (MWh)	1.037	977	1154
AC Power Profit (M€ $year^{-1}$)	0.822	0.781	0.922
Hydrogen Production (kg h^{-1})	19.2	27.0	21.5
Hydrogen Production Profit (M€ $year^{-1}$)	1.841	2.588	2.062

Table 6.10: Comparison of different scenarios for the payback analysis of the 1.744 MW CHHP system.

Scenario	1	2	3
Total Investment (M€)	20.05	20.39	22.17
Annual Consumption (M€)	0.550	0.589	0.615
Annual Production (M€)	2.941	3.660	3.294
Payback	8	6	8

Results show that the increase in hydrogen production has a more significant impact on the Payback than the available output power AC reducing it by 2 years. This result is rather predictable since when comparing the price established for each component, the price for pure hydrogen is 120 times higher than the one considered for electrical energy. Even though the amount of this last component is quite higher than the hourly production of hydrogen as expressed in Table 6.9 it still does not surpass the possible profit generated by this component. Lastly, by evaluating the investment for each scenario, one can observe that although increasing the hydrogen production increases the overall investment, it is not

as impactful as the investment performed when the power production is increased.

Furthermore, to evaluate the input conditions that allowed a Payback equal to or, ideally, below 5 years, graphic 6.1 relates this performance indicator with the U_f.

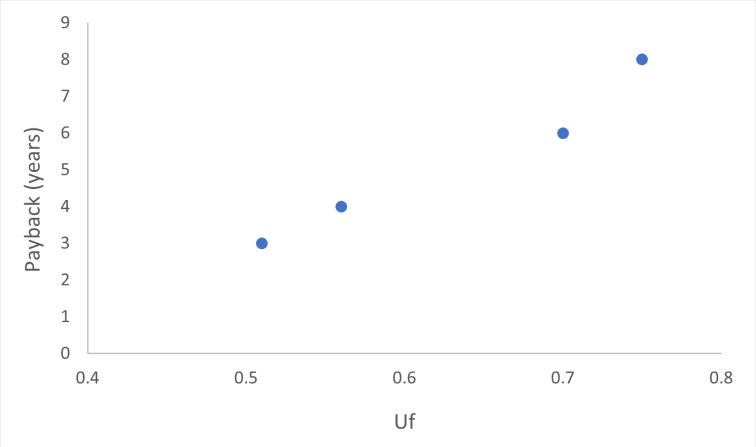

Figure 6.1: Effects of U_f on the Payback.

This first and most apparent conclusion with this graphic analysis is that the Payback reduces with the reduction of the U_f. From approximately a U_f of 0.60, the Payback is below 5 years. According to the tests executed for using a U_f of 0.56 allows to pay the initial investment in 4 years and 2 months while reducing the U_f to 0.51 already translates on Payback of 3 years and 8 months. The quantity of hydrogen produced daily, here discussed, varies between 461 to 1682 kg, which in comparison with the values presented in Table 5.4 is still lower than the convention SMR process on a large scale. Yet, it can surpass the electrolysis process and SMR process on a distributed scale, meaning that it is correctly placed in the values practiced in these industries. Besides, high U_f could cause SOFC anode re-oxidation, which affects the SOFC stack life expectancy and also reduces the partial pressure and Nernst potential. This causes a lower cell efficiency and power production, which ultimately increases the capital cost for a given power production [136].

Knowing that hydrogen production is determinant in the Payback, the price set for this component is also an essential factor to assess. As previously mentioned, the assumed value was quite conservative. The following graphic demonstrates how the variation in hydrogen price influences the Payback. For this purpose, three scenarios expressed in Figure 6.1 were chosen, two with a favorable payback (PB=3 and 4 years) and the other with an unfavorable payback (PB= 6 years).

The hydrogen price causes a greater impact in reducing the payback of the unfavorable scenario than in the other two scenarios. Although the hydrogen production on these two scenarios (1 354 kg day^{-1} and 1 682 kg day^{-1}) is higher than the other one (1 195 kg day^{-1}), the total investment in this last case

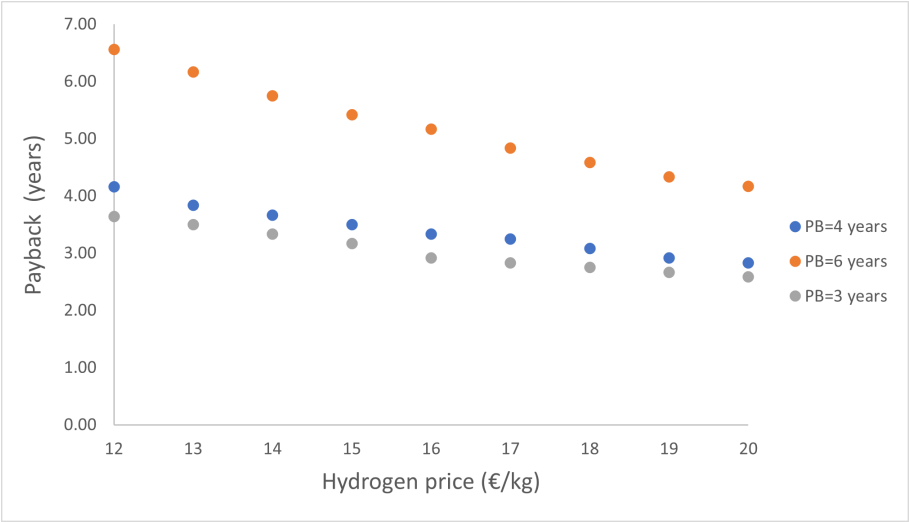

Figure 6.2: Effects of the price set for hydrogen on the Payback.

is between 1 to 2 M€ less expensive which can allow a faster recovery of the investment performed if the hydrogen price increases. Nevertheless, in order to consider a competitive price in the market, such as 15€/ kg of hydrogen produced, the unfavorable scenario still has a payback slightly above 5 years, hence the other two scenarios will be evaluated in further detail to choose the most suitable one for this project. Besides establishing the price of 15€ kg^{-1}, it was also taken into account that an investment in a new SOFC system would be executed every five years. The annual revenue for each scenario over the project time frame is presented below, taking the annual sales and operating costs into account. These parameters are all discriminated in Appendix C Tables C.5 to C.8. It should be mentioned that scenario in Fig. 6.3 corresponds to a total investment of 21.8 M€, while scenario in Fig. 6.4 translates a total investment of 21.1 M€.

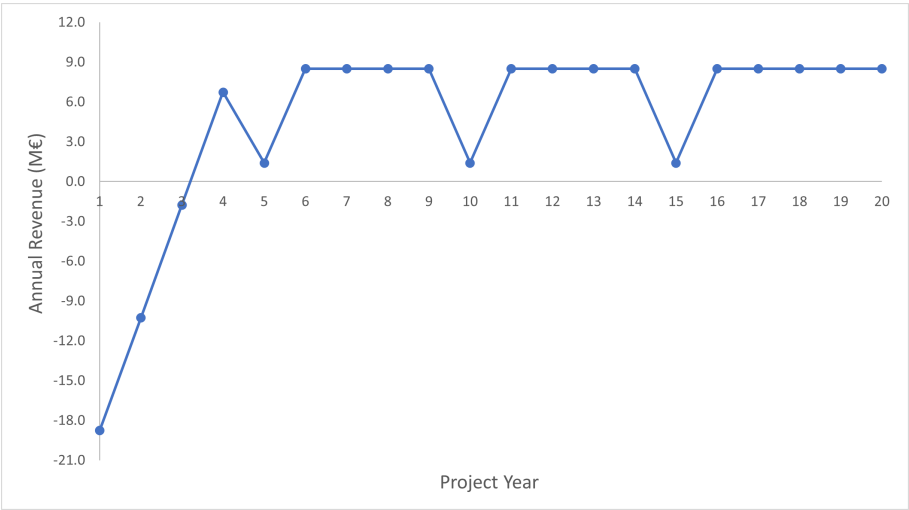

Figure 6.3: Revenue for the scenario with a payback of 3 years and 2 months.

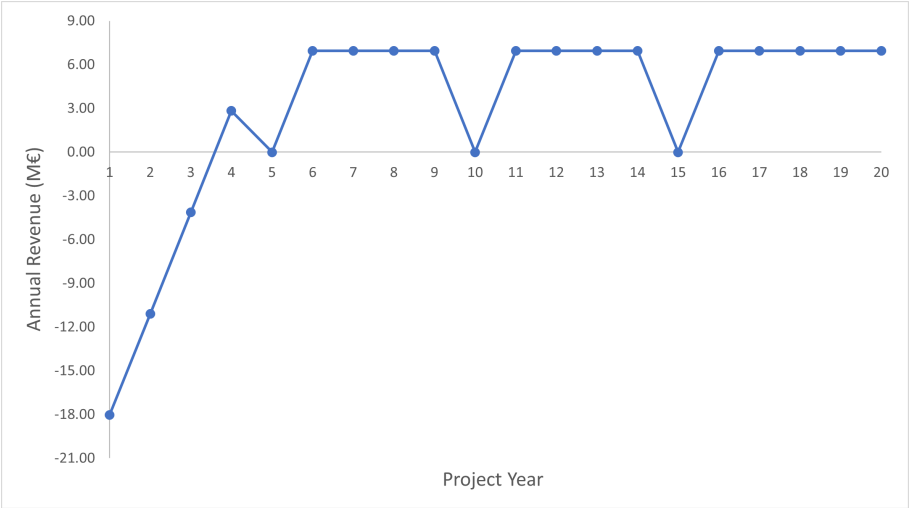

Figure 6.4: Revenue for the scenario with a payback of 3 years and 6 months.

By analyzing Figure 6.3 and 6.4 it is possible to observe a negative revenue in the first three years where the generated profit still does not outpace the total investment. In the following years there are periods were the revenue is constant which in Figure 6.3 corresponds to 8.50 M€ and in Figure 6.4 6.96 M€. The revenue shortfalls presented concern the years where the SOFC system should be replaced. This has a greater impact for the case represented in Figure 6.4 where revenue decreases for -6 518€ than in the case of Figure 6.3 where it only decreases for 1.404 M€. Even though it demands a slightly higher initial investment, it can be affirmed that the scenario with the highest revenue and which favorably balances the expenditure associated with the SOFC system is the one presented in Figure 6.3. Regarding the electrical energy available for the GTs auxiliary equipment, 677.23 kW can be displayed, meaning that 382.77 kW are imported from the REN grid. All input data regarding the optimum scenario chosen is in Appendix C, Table C.9.

With the economic analysis carried out, it was concluded that the production of high purity hydrogen presents a more significant impact on the profitability of the CHHP system than the electrical energy production, which is why it has become the main focus of discussion. However, producing electrical energy inside Sine's Refinery also presents economic benefits since there is no need to pay costly fees to access the REN grid. Finally, possible fiscal and investment support from the Portuguese Government and/or other organizations such as the European Union, associated with projects that promote environmental sustainability and clean energy valorization, were not considered. Nonetheless, it could have a very positive outcome on the economic analysis performed.

Chapter 7

Conclusions and Future Work

This thesis aimed to study the feasibility of a trigeneration (CHHP) system using SOFC. It could provide electrical energy for the GTs auxiliary equipment presented in the Cogeneration system already implemented in the Utility Plant and produce hydrogen with 99.999% purity for mobility applications. State-of-the-art regarding SOFC was also reviewed in further detail.

SOFC are high temperature fuel cells that accept a wide variety of fuels, for instance, hydrocarbons, which is a strong advantage compared to the other types of fuel cells. They are already quite exploited in CHP systems and off-grid power generation and can be used in the range of kW to MW. One highly acknowledge SOFC manufacturing company is Bloom Energy. The technology provided by this company was the one chosen to be applied in this project. They produce SOFC modules known as ”Servers” with an output power of 200-300kW. They can be combined, offering flexibility on the overall output power that easily reaches the MW scale.

The CHHP system was developed using Aspen Plus V11 software in order to evaluate its feasibility. Moreover, two distinct SOFC models (Approach 1 and 2) were applied to determine the cell voltage. Approach 1 determined 0.873 V, which corresponds to 1.140 MW. In comparison, with Approach 2 a cell voltage of 0.812 V was calculated corresponding to an output power AC of 1.060 MW, precisely the output for which the initial calculations implemented in Aspen Plus were conducted. It was possible to conclude that Approach 2 is more accurate than Approach 1, since it considers activation, ohmic polarization, and concentration losses with a temperate and pressure dependency, whilst Approach 1 is defined using semi-empirical equations. To validate the results obtained in Aspen Plus, the CHHP system developed was adjusted to the conditions of two case studies, [113, 105]. Regarding the electri-

cal power production, the results obtained for both cases presented a discrepancy below 10% between the implemented system and the values stated in the literature. The hydrogen production was also in accordance with the provided data. In Case Study 1, it reached the same value, while in Case Study 2, the model results indicate a daily production of 225.2 kg, which is close enough to the value stated by the literature, 229.2 kg. Hence, the input conditions which satisfy the desired output power of 1.067 MW and deliver a heat and hydrogen production of 3.03 MMBtu h^{-1} and 16.5 kg h^{-1}, respectively, are 10 kmol/h of fuel gas, 219.8 kmol h^{-1} of air, and 6.5 kmol h^{-1} of freshwater.

Lastly, an economic analysis with the input data and results stated above was performed. At this stage, the auto-consumption of the leading equipment was taken into account, noticing that only 603.5 kW are available to be delivered to the GTs auxiliary equipment. Therefore, in the perspective of reaching the desired electrical energy production, input conditions were once again adapted. Considering 15.23 kmol h^{-1} of fuel gas, 357.1 kmol h^{-1} of air and 10 kmol h^{-1} of freshwater, the AC output power is 1.744 MW, and 1.030 MW are supplied to the GTs auxiliary equipment. A total investment of 20.045 M€ was determined. Afterward, to analyse the economic performance associated with the project under evaluation, the Payback was calculated. Ideally, this indicator ought to be less than 5 years due to the SOFCs lifetime. For the proposed scenario, the Payback is 8 years which is far from being suitable. For this reason, increasing the profit, whether from an increase in the electrical energy produced or hydrogen, was tested. It was observed that this last one had a more significant impact in reducing the Payback in comparison with the electrical energy production, mainly due to the difference in the price set for both. Thus, from an economic point of view, favoring a scenario that values the hydrogen overproduction is much more profitable, despite causing an increase in the auto-consumption of the equipment and consequently a reduction in the electrical energy distributed. Considering 22.5 kmol h^{-1} of fuel gas, 19.5 kmol h^{-1} of water and 357.1 kmol h^{-1} air and setting the price for hydrogen on 15€ kg^{-1} allows a Payback of 3 years and 2 months with yearly revenue of 8.496 M€ for a total investment of 21.8 M€. Although in the years where the SOFC system is replaced the revenue value drops, it is still positive and corresponds to 1.404 M€. For this scenario, the hydrogen production reaches 70.1 kg/h (1 682 kg per day) and the electrical energy available for the cogeneration system is 677 kW.

In conclusion, it was possible to confirm that the SOFC applied to the trigeneration concept is attainable from the technical point of view and an interesting investment with strong hypotheses of profitability, especially in the current market where efforts are coming together to change for a hydrogen mobility paradigm. Besides, hydrogen fuel cell vehicles present the advantage to achieve between 80 and 112 km kg^{-1} of hydrogen, which is almost double the fuel economy, in kilometers per gallon of gasoline, compared to a gasoline powered car [105]. In addition, it reduces the amount of CO_2 emissions in comparison to conventional power plants, due to the SOFC system and the exploitation of the fuel gas,

eliminating discharges on the flare.

Regarding possible future work on this subject, the literature that combines this type of system with SOFCs is still quite scarce, hindering the possibility of comparing and validating results. Hence, besides developing more studies on this matter, its application on a pilot scale would be an interesting starting point before applying to the dimension here discussed. As mentioned in the literature review, improvements in reducing SOFC operating temperature may exclude the need to use such resistant materials, reducing its cost, causing a massive impact on the overall investment regarding the trigeneration system. Also, to reduce operational costs, increasing SOFC lifetime is crucial to be competitive with traditional power generation technologies. This is feasible if a low power density and low fuel utilization are employed [137]. Lastly, the use of MCFCs instead of SOFCs should also be discussed. Although it is stated that SOFCs allow a higher overall efficiency than MCFC, and that was the main reason why they were excluded, these are already applied in the market in trigeneration systems such as the SureSource Hydrogen^{TM}. This plant corresponds to a 2.3 MW platform that produces 1 200 kg of hydrogen per day in addition to the electricity, thermal energy, and water generated by the fuel cell [138]. On further studies, the possibility of adapting this system to the conditions at Sine's Refinery also presents a compelling interest since the constraint of not being already applied on an industrial scale is avoided.

Bibliography

[1] A. M. Abdalla, S. Hossain, P. M. Petra, M. Ghasemi, and A. K. Azad, "Achievements and trends of solid oxide fuel cells in clean energy field: a perspective review," *Frontiers in Energy*, vol. 14, no. 2, pp. 359–382, 2020.

[2] X. Zhang, S. Chan, G. Li, H. Ho, J. Li, and Z. Feng, "A review of integration strategies for solid oxide fuel cells," *Journal of Power Sources*, vol. 195, no. 3, pp. 685–702, 2010.

[3] T. Morgan, "The hydrogen economy: A non-technical review," 2006.

[4] M. Reisert, A. Aphale, and P. Singh, "Solid oxide electrochemical systems: Material degradation processes and novel mitigation approaches," *Materials*, vol. 11, no. 11, p. 2169, 2018.

[5] S. Mekhilef, R. Saidur, and A. Safari, "Comparative study of different fuel cell technologies," *Renewable and Sustainable Energy Reviews*, vol. 16, no. 1, pp. 981–989, 2012.

[6] O. Z. Sharaf and M. F. Orhan, "An overview of fuel cell technology: Fundamentals and applications," *Renewable and sustainable energy reviews*, vol. 32, pp. 810–853, 2014.

[7] B. Cook, "Introduction to fuel cells and hydrogen technology," *Engineering science and education journal*, vol. 11, no. 6, pp. 205–216, 2002.

[8] R. M. Ormerod, "Solid oxide fuel cells," *Chemical Society Reviews*, vol. 32, no. 1, pp. 17–28, 2003.

[9] A. Therdthianwong, P. Saenwiset, and S. Therdthianwong, "Cathode catalyst layer design for proton exchange membrane fuel cells," *Fuel*, vol. 91, no. 1, pp. 192–199, 2012.

[10] K. Sopian and W. R. W. Daud, "Challenges and future developments in proton exchange membrane fuel cells," *Renewable energy*, vol. 31, no. 5, pp. 719–727, 2006.

[11] "Comparison of Fuel Cell Technologies." `https://www.energy.gov/eere/fuelcells/comparison-fuel-cell-technologies`. [Online; Accessed 28-July-2021].

[12] K. Kordesch, "Alkaline fuel cells applications, innovative energy technology," *Austria: Institute of High Voltage Engineering, U Graz*, 1999.

[13] J. Larminie, A. Dicks, and M. S. McDonald, *Fuel cell systems explained*, vol. 2. J. Wiley Chichester, UK, 2003.

[14] K. Chudej, M. Bauer, H. J. Pesch, and K. Schittkowski, "Numerical simulation of a molten carbonate fuel cell by partial differential algebraic equations," in *From Nano to Space*, pp. 57–70, Springer, 2008.

[15] W. He, "Dynamic performance of a reformer for molten carbonate fuel cell power-generation systems," *Fuel processing technology*, vol. 53, no. 1-2, pp. 99–113, 1997.

[16] R. J. Remick, D. Wheeler, and P. Singh, "Mcfc and pafc r&d workshop summary report," 2010.

[17] "Fuel Cells Types." `http://www.nfcrc.uci.edu/Fuel_Cells_Types.html`. [Online; Accessed 28-July-2021].

[18] "Types of Fuel Cells." `https://www.energy.gov/eere/fuelcells/types-fuel-cells`. [Online; Accessed 28-July-2021].

[19] S. C. Singhal, "Advances in solid oxide fuel cell technology," *Solid state ionics*, vol. 135, no. 1-4, pp. 305–313, 2000.

[20] J. Will, A. Mitterdorfer, C. Kleinlogel, D. Perednis, and L. Gauckler, "Fabrication of thin electrolytes for second-generation solid oxide fuel cells," *Solid State Ionics*, vol. 131, no. 1-2, pp. 79–96, 2000.

[21] M. Sahibzada, B. Steele, D. Barth, R. Rudkin, and I. Metcalfe, "Operation of solid oxide fuel cells at reduced temperatures," *Fuel*, vol. 78, no. 6, pp. 639–643, 1999.

[22] K. Tanaka, C. Wen, and K. Yamada, "Design and evaluation of combined cycle system with solid oxide fuel cell and gas turbine," *Fuel*, vol. 79, no. 12, pp. 1493–1507, 2000.

[23] X. Zhang, S. Chan, G. Li, H. Ho, J. Li, and Z. Feng, "A review of integration strategies for solid oxide fuel cells," *Journal of Power Sources*, vol. 195, no. 3, pp. 685–702, 2010.

[24] P. Jienkulsawad, D. Saebea, Y. Patcharavorachot, S. Kheawhom, and A. Arpornwichanop, "Analysis of a solid oxide fuel cell and a molten carbonate fuel cell integrated system with different configurations," *International Journal of Hydrogen Energy*, vol. 43, no. 2, pp. 932–942, 2018.

[25] I. Malico, A. P. Carvalhinho, and J. Tenreiro, "Design of a trigeneration system using a high-temperature fuel cell," *International Journal of Energy Research*, vol. 33, no. 2, pp. 144–151, 2009.

[26] "The Green Growth Commitment and The Green Taxation Reform." `https://www.crescimentoverde.gov.pt/wp-content/uploads/2014/10/2014_12_05_`

Portugal-green-taxation-reforma-and-green-growth-deal.pdf, 2014. [Online; Accessed 29-July-2021].

[27] "Galp joins the Hydrogen Council and mulls projects to promote hydrogen economy in Portugal." https://www.galp.com/corp/en/media/press-releases/press-release/id/1043/galp-joins-the-hydrogen-council-and-mulls-projects-to-promote-hydrogen-economy-in-portugal. [Online; Accessed 24-July-2021].

[28] Galp, *Manual Descritivo da Fábrica de Utilidades*.

[29] C. Mendonça, A. Ferreira, and D. M. Santos, "Towards the commercialization of solid oxide fuel cells: Recent advances in materials and integration strategies," *Fuels*, vol. 2, no. 4, pp. 393–419, 2021.

[30] A. Stambouli and E. Traversa, "Solid oxide fuel cells (sofcs): a review of an environmentally clean and efficient source of energy," *Renewable and Sustainable Energy Reviews*, vol. 6, no. 5, pp. 433–455, 2002.

[31] A. Abdalla, S. Hossain, A. Azad, P. Petra, F. Begum, S. Eriksson, and A. Azad, "Nanomaterials for solid oxide fuel cells: A review," *Renewable and Sustainable Energy Reviews*, vol. 82, p. 368, 02 2018.

[32] H. Shi, C. Su, R. Ran, J. Cao, and Z. Shao, "Electrolyte materials for intermediate-temperature solid oxide fuel cells," *Progress in Natural Science: Materials International*, vol. 30, no. 6, pp. 764–774, 2020.

[33] D. Sarantaridis and A. Atkinson, "Mechanical modeling of redox cycling damage in solid oxide fuel cells," *Proceedings of the 7th European Solid Oxide Fuel Cell Forum*, p. P0728, 01 2006.

[34] E. Months, A. Date, M. Gandiglio, T. Hakala, and E. Fontell, "Comsos "commercial-scale sofc systems"," pp. 1–11, 2019.

[35] A. Faes, A. Hessler-Wyser, A. Zryd, and J. Van Herle, "A review of redox cycling of solid oxide fuel cells anode," *Membranes*, vol. 2, no. 3, pp. 585–664, 2012.

[36] N. Laosiripojana, W. Wiyaratn, W. Kiatkittipong, A. Arpornwichanop, A. Soottitantawat, and S. Assabumrungrat, "Reviews on solid oxide fuel cell technology," *Engineering Journal*, pp. 65–84, February 2009.

[37] A. Tesfai, P. Connor, J. Nairn, and J. T. S. Irvine, "Thermal Cycling Evaluation of Rolled Tubular Solid Oxide Fuel Cells," *Journal of Fuel Cell Science and Technology*, vol. 8, 09 2011.

[38] A. M. Hussain and E. D. Wachsman, “Liquids-to-power using low-temperature solid oxide fuel cells,” *Energy Technology*, vol. 7, no. 1, pp. 20–32, 2019.

[39] A. Choudhury, H. Chandra, and A. Arora, “Application of solid oxide fuel cell technology for power generation—A review,” *Renewable and Sustainable Energy Reviews*, vol. 20, pp. 430–442, 2013.

[40] D. J. Brett, A. Atkinson, N. P. Brandon, and S. J. Skinner, “Intermediate temperature solid oxide fuel cells,” *Chemical Society Reviews*, vol. 37, no. 8, pp. 1568–1578, 2008.

[41] Y. Lyu, J. Xie, D. Wang, and J. Wang, “Review of cell performance in solid oxide fuel cells,” *Journal of Materials Science*, vol. 55, no. 17, pp. 7184–7207, 2020.

[42] K. Patil, *Chemistry of nanocrystalline oxide materials: combustion synthesis, properties and applications*. World Scientific, 2008.

[43] Y. Jiang and A. V. Virkar, “A high performance, anode-supported solid oxide fuel cell operating on direct alcohol,” *Journal of the Electrochemical Society*, vol. 148, no. 7, p. A706, 2001.

[44] P. Satardekar, D. Montinaro, and V. M. Sglavo, “Fe-doped ysz electrolyte for the fabrication of metal supported-sofc by co-sintering,” *Ceramics International*, vol. 41, no. 8, pp. 9806–9812, 2015.

[45] B. S. Prakash, R. Pavitra, S. S. Kumar, and S. Aruna, “Electrolyte bi-layering strategy to improve the performance of an intermediate temperature solid oxide fuel cell: A review,” *Journal of Power Sources*, vol. 381, pp. 136–155, 2018.

[46] T. Shimonosono, Y. Hirata, S. Sameshima, and T. Horita, “Electronic conductivity of la-doped ceria ceramics,” *Journal of the American Ceramic Society*, vol. 88, no. 8, pp. 2114–2120, 2005.

[47] J. Van Herle, D. Seneviratne, and A. McEvoy, “Lanthanide co-doping of solid electrolytes: Ac conductivity behaviour,” *Journal of the European Ceramic Society*, vol. 19, no. 6-7, pp. 837–841, 1999.

[48] N. Jaiswal, K. Tanwar, R. Suman, D. Kumar, S. Upadhyay, and O. Parkash, “A brief review on ceria based solid electrolytes for solid oxide fuel cells,” *Journal of Alloys and Compounds*, vol. 781, pp. 984–1005, 2019.

[49] C. Tealdi, L. Malavasi, C. Ritter, G. Flor, and G. Costa, “Lattice effects in cubic la2mo2o9: Effect of vacuum and correlation with transport properties,” *Journal of Solid State Chemistry*, vol. 181, no. 3, pp. 603–610, 2008.

[50] T. Ishihara, H. Matsuda, and Y. Takita, “Doped lagao3 perovskite type oxide as a new oxide ionic conductor,” *Journal of the American chemical society*, vol. 116, no. 9, pp. 3801–3803, 1994.

[51] M. Morales, J. Roa, J. Tartaj, and M. Segarra, "A review of doped lanthanum gallates as electrolytes for intermediate temperature solid oxides fuel cells: From materials processing to electrical and thermo-mechanical properties," *Journal of the European Ceramic Society*, vol. 36, no. 1, pp. 1–16, 2016.

[52] A. Solovyev, A. V. Shipilova, I. V. Ionov, A. N. Kovalchuk, S. Rabotkin, and V. Oskirko, "Magnetron-sputtered ysz and cgo electrolytes for sofc," *Journal of Electronic Materials*, vol. 45, no. 8, pp. 3921–3928, 2016.

[53] N. Ito, M. Iijima, K. Kimura, and S. Iguchi, "New intermediate temperature fuel cell with ultra-thin proton conductor electrolyte," *Journal of Power Sources*, vol. 152, pp. 200–203, 2005.

[54] Y. Zhang, R. Knibbe, J. Sunarso, Y. Zhong, W. Zhou, Z. Shao, and Z. Zhu, "Solid-oxide fuel cells: Recent progress on advanced materials for solid-oxide fuel cells operating below 500° c (adv. mater. 48/2017)," *Advanced Materials*, vol. 29, no. 48, p. 1770345, 2017.

[55] W. Vielstich, A. Lamm, and H. Gasteiger, "Handbook of fuel cells. fundamentals, technology, applications," 2003.

[56] S. Badwal, "Materials for solid oxide fuel cells," in *Materials Forum*, vol. 21, pp. 187–224, 1997.

[57] B. C. Steele and A. Heinzel, "Materials for fuel-cell technologies," in *Materials for sustainable energy: a collection of peer-reviewed research and review articles from nature publishing group*, pp. 224–231, World Scientific, 2011.

[58] S. M. Haile, "Materials for fuel cells," *Materials today*, vol. 6, no. 3, pp. 24–29, 2003.

[59] J. C. Mah, A. Muchtar, M. R. Somalu, and M. J. Ghazali, "Metallic interconnects for solid oxide fuel cell: A review on protective coating and deposition techniques," *International Journal of Hydrogen Energy*, vol. 42, no. 14, pp. 9219–9229, 2017.

[60] I. Sreedhar, B. Agarwal, P. Goyal, and S. A. Singh, "Recent advances in material and performance aspects of solid oxide fuel cells," *Journal of Electroanalytical Chemistry*, vol. 848, p. 113315, 2019.

[61] Z. Yang, K. S. Weil, D. M. Paxton, and J. W. Stevenson, "Selection and evaluation of heat-resistant alloys for sofc interconnect applications," *Journal of the Electrochemical Society*, vol. 150, no. 9, p. A1188, 2003.

[62] Z. Yang, G.-G. Xia, X.-H. Li, and J. W. Stevenson, "(mn, co) 3o4 spinel coatings on ferritic stainless steels for sofc interconnect applications," *International Journal of Hydrogen Energy*, vol. 32, no. 16, pp. 3648–3654, 2007.

[63] J. Wu and X. Liu, “Recent development of sofc metallic interconnect,” *Journal of materials science and technology*, vol. 26, no. 4, pp. 293–305, 2010.

[64] Z. Wang, N. Zhang, J. Qiao, K. Sun, and P. Xu, “Improved sofc performance with continuously graded anode functional layer,” *Electrochemistry Communications*, vol. 11, no. 6, pp. 1120–1123, 2009.

[65] J.-J. Lee, H. Moon, H.-G. Park, D. I. Yoon, and S.-H. Hyun, “Applications of nano-composite materials for improving the performance of anode-supported electrolytes of sofcs,” *International Journal of Hydrogen Energy*, vol. 35, no. 2, pp. 738–744, 2010.

[66] S. Afroze, A. Karim, Q. Cheok, S. Eriksson, and A. K. Azad, “Latest development of double perovskite electrode materials for solid oxide fuel cells: a review,” *Frontiers in Energy*, vol. 13, no. 4, pp. 770–797, 2019.

[67] Y. Chen, Y. Bu, B. Zhao, Y. Zhang, D. Ding, R. Hu, T. Wei, B. Rainwater, Y. Ding, F. Chen, *et al.*, “A durable, high-performance hollow-nanofiber cathode for intermediate-temperature fuel cells,” *Nano Energy*, vol. 26, pp. 90–99, 2016.

[68] L. Shu, J. Sunarso, S. S. Hashim, J. Mao, W. Zhou, and F. Liang, “Advanced perovskite anodes for solid oxide fuel cells: A review,” *International Journal of Hydrogen Energy*, vol. 44, no. 59, pp. 31275–31304, 2019.

[69] Y. Kim, J.-H. Kim, A. Huq, M. Paranthaman, and A. Manthiram, “(y0. 5in0. 5) ba (co, zn) 4o7 cathodes with superior high-temperature phase stability for solid oxide fuel cells,” *Journal of Power Sources*, vol. 214, pp. 7–14, 2012.

[70] C. Sun, R. Hui, and J. Roller, “Cathode materials for solid oxide fuel cells: a review,” *Journal of Solid State Electrochemistry*, vol. 14, no. 7, pp. 1125–1144, 2010.

[71] B. McCarthy, L. R. Pederson, Y. Chou, X.-D. Zhou, W. Surdoval, and L. Wilson, “Low-temperature sintering of lanthanum strontium manganite-based contact pastes for sofcs,” *Journal of power sources*, vol. 180, no. 1, pp. 294–300, 2008.

[72] D. L. Meixner and R. A. Cutler, “Sintering and mechanical characteristics of lanthanum strontium manganite,” *Solid State Ionics*, vol. 146, no. 3-4, pp. 273–284, 2002.

[73] N. Q. Minh, “Ceramic fuel cells,” *Journal of the American Ceramic Society*, vol. 76, no. 3, pp. 563–588, 1993.

[74] S. Lion and W. Worrell, “Electrical properties of novel mixed-conducting oxides,” *Applied Physics A*, vol. 49, no. 1, pp. 25–31, 1989.

[75] A. Gholizadeh, "The effects of a/b-site substitution on structural, redox and catalytic properties of lanthanum ferrite nanoparticles," *Journal of Materials Research and Technology*, vol. 8, no. 1, pp. 457–466, 2019.

[76] S.-e. Hou, J. A. Alonso, and J. B. Goodenough, "Co-free, iron perovskites as cathode materials for intermediate-temperature solid oxide fuel cells," *Journal of Power Sources*, vol. 195, no. 1, pp. 280–284, 2010.

[77] D. Chen, C. Chen, F. Dong, Z. Shao, and F. Ciucci, "Cobalt-free polycrystalline ba0. 95la0. 05feo3-δ thin films as cathodes for intermediate-temperature solid oxide fuel cells," *Journal of Power Sources*, vol. 250, pp. 188–195, 2014.

[78] S. S. Hashim, F. Liang, W. Zhou, and J. Sunarso, "Cobalt-free perovskite cathodes for solid oxide fuel cells," *ChemElectroChem*, vol. 6, no. 14, pp. 3549–3569, 2019.

[79] L. Yang, S. Wang, K. Blinn, M. Liu, Z. Liu, Z. Cheng, and M. Liu, "Enhanced sulfur and coking tolerance of a mixed ion conductor for sofcs: Bazr0.1ce0. 7y0. 2–xybxo3–δ," *Science*, vol. 326, no. 5949, pp. 126–129, 2009.

[80] M. Rokni, "Thermodynamic analysis of an integrated solid oxide fuel cell cycle with a rankine cycle," *Energy conversion and management*, vol. 51, no. 12, pp. 2724–2732, 2010.

[81] S. Chan, C. Low, and O. Ding, "Energy and exergy analysis of simple solid-oxide fuel-cell power systems," *Journal of power sources*, vol. 103, no. 2, pp. 188–200, 2002.

[82] "SOFC Stack - Energy Conversion Devices." `https://global.kyocera.com/prdct/ecd/sofc/`. [Online; Accessed 19-April-2021].

[83] "KYOCERA Develops Industry's First 3-Kilowatt Solid-Oxide Fuel Cell for Institutional Cogeneration; Most efficient SOFC on the market using proprietary ceramic technology." `https://global.kyocera.com/news-archive/2017/0702_bnfo.html`. [Online; Accessed 19-April-2021].

[84] "Powering the Future of Clean Energy." `https://www.bloomenergy.com/company/`. [Online; Accessed 5-June-2021].

[85] M. Andersson and J. Froitzheim, "Technology review – solid oxide cells 2019," 2019.

[86] X. Zhang, "Current status of stationary fuel cells for coal power generation," *Clean Energy*, vol. 2, no. 2, pp. 126–139, 2018.

[87] "Who we are." `https://www.fch.europa.eu/page/who-we-are`. [Online; Accessed 19-April-2021].

[88] "Workshop Industrial application of SOFC systems- DEMOSOFC project." https://www.fch.europa.eu/event/workshop-industrial-application-sofc-systems-demosofc-projec. [Online; Accessed 19-April-2021].

[89] A. Mehr, A. Lanzini, M. Santarelli, and M. A. Rosen, "Polygeneration systems based on high temperature fuel cell (mcfc and sofc) technology: System design, fuel types, modeling and analysis approaches," *Energy*, vol. 228, p. 120613, 2021.

[90] "Communication from the commission to the european parliament, the council, the european economic and social committee and the committee of the regions: An eu strategy on heating and cooling," 2016.

[91] M. Jradi and S. Riffat, "Tri-generation systems: Energy policies, prime movers, cooling technologies, configurations and operation strategies," *Renewable and Sustainable Energy Reviews*, vol. 32, pp. 396–415, 2014.

[92] H. Al Moussawi, F. Fardoun, and H. Louahlia-Gualous, "Review of tri-generation technologies: Design evaluation, optimization, decision-making, and selection approach," *Energy Conversion and Management*, vol. 120, pp. 157–196, 2016.

[93] H. Ozcan and I. Dincer, "Performance evaluation of an sofc based trigeneration system using various gaseous fuels from biomass gasification," *International journal of hydrogen energy*, vol. 40, no. 24, pp. 7798–7807, 2015.

[94] M. Mortazaei and M. Rahimi, "A comparison between two methods of generating power, heat and refrigeration via biomass based solid oxide fuel cell: A thermodynamic and environmental analysis," *Energy conversion and management*, vol. 126, pp. 132–141, 2016.

[95] E. Gholamian, V. Zare, and S. M. Mousavi, "Integration of biomass gasification with a solid oxide fuel cell in a combined cooling, heating and power system: a thermodynamic and environmental analysis," *international journal of hydrogen energy*, vol. 41, no. 44, pp. 20396–20406, 2016.

[96] V. Palomba, M. Prestipino, and A. Galvagno, "Tri-generation for industrial applications: Development of a simulation model for a gasification-sofc based system," *International Journal of Hydrogen Energy*, vol. 42, no. 46, pp. 27866–27883, 2017.

[97] R. Segurado, S. Pereira, D. Correia, and M. Costa, "Techno-economic analysis of a trigeneration system based on biomass gasification," *Renewable and Sustainable Energy Reviews*, vol. 103, pp. 501–514, 2019.

[98] M. Burer, K. Tanaka, D. Favrat, and K. Yamada, "Multi-criteria optimization of a district cogeneration plant integrating a solid oxide fuel cell–gas turbine combined cycle, heat pumps and chillers," *Energy*, vol. 28, no. 6, pp. 497–518, 2003.

[99] F. A. Al-Sulaiman, I. Dincer, and F. Hamdullahpur, "Energy analysis of a trigeneration plant based on solid oxide fuel cell and organic rankine cycle," *International Journal of Hydrogen Energy*, vol. 35, no. 10, pp. 5104–5113, 2010.

[100] F. A. Al-Sulaiman, F. Hamdullahpur, and I. Dincer, "Performance comparison of three trigeneration systems using organic rankine cycles," *Energy*, vol. 36, no. 9, pp. 5741–5754, 2011.

[101] D. Yu, Y. Mao, B. Gu, S. Nojavan, K. Jermsittiparsert, and M. Nasseri, "A new lqg optimal control strategy applied on a hybrid wind turbine/solid oxide fuel cell/in the presence of the interval uncertainties," *Sustainable Energy, Grids and Networks*, vol. 21, p. 100296, 2020.

[102] C. Weber, M. Koyama, and S. Kraines, "Co2-emissions reduction potential and costs of a decentralized energy system for providing electricity, cooling and heating in an office-building in tokyo," *Energy*, vol. 31, no. 14, pp. 3041–3061, 2006.

[103] H. Al Moussawi, F. Fardoun, and H. Louahlia, "Selection based on differences between cogeneration and trigeneration in various prime mover technologies," *Renewable and Sustainable Energy Reviews*, vol. 74, pp. 491–511, 2017.

[104] K. Hemmes, L. Kamp, A. Vernay, and G. De Werk, "A multi-source multi-product internal reforming fuel cell energy system as a stepping stone in the transition towards a more sustainable energy and transport sector," *International Journal of hydrogen energy*, vol. 36, no. 16, pp. 10221–10227, 2011.

[105] W. Becker, R. Braun, M. Penev, and M. Melaina, "Design and technoeconomic performance analysis of a 1 mw solid oxide fuel cell polygeneration system for combined production of heat, hydrogen, and power," *Journal of Power Sources*, vol. 200, pp. 34–44, 2012.

[106] A. Fernandes, T. Woudstra, A. Van Wijk, L. Verhoef, and P. Aravind, "Fuel cell electric vehicle as a power plant and sofc as a natural gas reformer: An exergy analysis of different system designs," *Applied Energy*, vol. 173, pp. 13–28, 2016.

[107] J. Brouwer, A. Azizi, *et al.*, "Thermodynamic and dynamic assessment of solid oxide fuel cell hybrid systems for use in locomotives," tech. rep., United States. Department of Transportation. Federal Railroad Administration, 2019.

[108] "BLOOM ENERGY SERVER ES5-250KW." `https://www.bloomenergy.com/resource/bloom-energy-server-es5-250kw/`. [Online; Accessed 2-August-2021].

[109] S. R. Pandya, V. M. Shah, and S. D. Shah, “Green manufacturing of electricity using sofc based bloom energy servertm,”

[110] M. K. Abd Hamid, “Hysys®: An introduction to chemical engineering simulation,” 2007.

[111] M. Mehrpooya, M. Sadeghzadeh, A. Rahimi, and M. Pouriman, “Technical performance analysis of a combined cooling heating and power (cchp) system based on solid oxide fuel cell (sofc) technology–a building application,” *Energy Conversion and Management*, vol. 198, p. 111767, 2019.

[112] I. EG&G Technical Services, “Handbook, fuel cell,” *US Department of Energy, Office of Fossil Energy, National Energy Technology Laboratory-Morgantown, West Virginia*, 2004.

[113] D. Steward, M. Penev, G. Saur, W. Becker, and J. Zuboy, “Fuel cell power model version 2: Startup guide, system designs, and case studies. modeling electricity, heat, and hydrogen generation from fuel cell-based distributed energy systems,” tech. rep., National Renewable Energy Lab.(NREL), Golden, CO (United States), 2013.

[114] P. Pianko-Oprych and M. Palus, “Simulation of sofcs based power generation system using aspen,” *Polish Journal of Chemical Technology*, vol. 19, no. 4, 2017.

[115] A. Lanzini, M. Santarelli, and A. Viola, “Process modelling of a biogas-fed sofc-orc hybrid system,”

[116] P. Spath, A. Aden, T. Eggeman, M. Ringer, B. Wallace, and J. Jechura, “Biomass to hydrogen production detailed design and economics utilizing the battelle columbus laboratory indirectly-heated gasifier,” tech. rep., National Renewable Energy Lab., Golden, CO (US), 2005.

[117] S. Campanari, “Thermodynamic model and parametric analysis of a tubular sofc module,” *Journal of Power Sources*, vol. 92, no. 1, pp. 26–34, 2001.

[118] S. Masciandaro, M. Torrell, P. Leone, and A. Tarancón, “Three-dimensional printed yttria-stabilized zirconia self-supported electrolytes for solid oxide fuel cell applications,” *Journal of the European Ceramic Society*, vol. 39, no. 1, pp. 9–16, 2019.

[119] W. Doherty, A. Reynolds, and D. Kennedy, “Modelling and simulation of a biomass gasification-solid oxide fuel cell combined heat and power plant using aspen plus,” 2009.

[120] R. Bove, P. Lunghi, and N. M. Sammes, “Sofc mathematic model for systems simulations. part one: from a micro-detailed to macro-black-box model,” *International Journal of Hydrogen Energy*, vol. 30, no. 2, pp. 181–187, 2005.

[121] P. Costamagna, A. Selimovic, M. Del Borghi, and G. Agnew, “Electrochemical model of the integrated planar solid oxide fuel cell (ip-sofc),” *Chemical Engineering Journal*, vol. 102, no. 1, pp. 61–69, 2004.

[122] R. O'hayre, S.-W. Cha, W. Colella, and F. B. Prinz, *Fuel cell fundamentals*. John Wiley & Sons, 2016.

[123] P. Lisbona, A. Corradetti, R. Bove, and P. Lunghi, "Analysis of a solid oxide fuel cell system for combined heat and power applications under non-nominal conditions," *Electrochimica Acta*, vol. 53, no. 4, pp. 1920–1930, 2007.

[124] S. C. Light, *Integrated Resource Plan*. Seattle City Light, Integrated Resource Planning, 2010.

[125] W. Zhang, E. Croiset, P. L. Douglas, M. Fowler, and E. Entchev, "Simulation of a tubular solid oxide fuel cell stack using aspenplustm unit operation models," *Energy Conversion and Management*, vol. 46, no. 2, pp. 181–196, 2005.

[126] K. Fehrenbacher, "10 things you should know about Bloom Energy's IPO." https://www.greenbiz.com/article/10-things-you-should-know-about-bloom-energys-ipo, 2018. [Online; Accessed 15-August-2021].

[127] J. Kagan, "Payback Period." https://www.investopedia.com/terms/p/paybackperiod.asp, 2021. [Online; Accessed 17-August-2021].

[128] J. M. Reis, "Estimativa do Investimento e Avaliação Económico-Financeira do Projecto de uma Nova Fábrica," 2020.

[129] K. Gerdes, E. Grol, D. Keairns, and R. Newby, "Integrated gasification fuel cell performance and cost assessment," *National Energy Technology Laboratory, US Department of Energy*, pp. 1–26, 2009.

[130] J. M. Reis, "Driving with H2: Hydrogen cars." https://h2.live/en/wasserstoffautos/. [Online; Accessed 18-August-2021].

[131] R. Sousa, "Frotas automóveis movidas a hidrogénio." https://fleetmagazine.pt/2018/10/09/opiniao-fuel-cell-hidrogenio/, 2018. [Online; Accessed 18-August-2021].

[132] P. F. P. M. T. C. Hugo Santos, Nuno Silva, "Trigeração com produção de hidrogénio," 2019/19.

[133] A. Ghazouani, W. Xia, M. Ben Jebli, and U. Shahzad, "Exploring the role of carbon taxation policies on co_2 emissions: Contextual evidence from tax implementation and non-implementation european countries," *Sustainability*, vol. 12, no. 20, 2020.

[134] "CO2 Emissions per kWh of Electricity Generated in France." https://www.rte-france.com/en/eco2mix/co2-emissions, 2021. [Online; Accessed 18-August-2021].

[135] "Product Datasheet: Energy Server 5," 2019.

[136] H. Chen, C. Yang, N. Zhou, N. Farida Harun, D. Oryshchyn, and D. Tucker, "High efficiencies with low fuel utilization and thermally integrated fuel reforming in a hybrid solid oxide fuel cell gas turbine system," *Applied Energy*, vol. 272, p. 115160, 2020.

[137] "Improving the durability of solid oxide fuel cells (SOFC) stacks." `https://cordis.europa.eu/article/id/80177-improving-the-durability-of-solid-oxide-fuel-cells-sofc-stacks`, 2005. [Online; Accessed 2-September-2021].

[138] "FuelCell Energy 2020 Annual Report," 2020.

[139] "Equipment Costs: Plant Design and Economics for Chemical Engineers, 5th Edition." `http://www.mhhe.com/engcs/chemical/peters/data/`. [Online; Accessed 20-August-2021].

Appendix A

Aspen Implementation

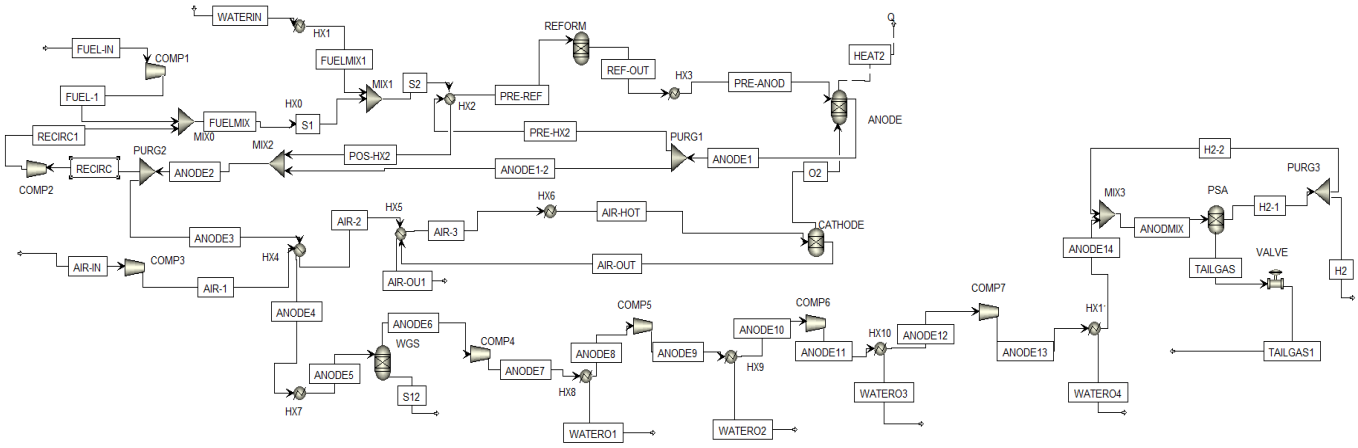

Figure A.1: Flowsheet of CHHP Process simulation.

Appendix B

Results and Discussion

Table B.1: Data from Aspen Plus.

Pressure Anode	110 000	Pa
PP(H_2)	19 858	Pa
PP(H_2O)	57 349	Pa
PP(O_2)	112 000	Pa

Table B.2: Results obtained for Approach 1.

V_{ref}	700.0	mV
ΔV_p	2.10	mV
ΔV_t	32	mV
ΔV_{anode}	62.6	mV
$\Delta V_{cathode}$	76.2	mV
V_c	0.873	V
I	1484.6	kA
P_{DC}	1.296	MW
P_{AC}	1.140	MW

Table B.3: Results obtained for Approach 2.

OCV_{exp}	0.813	mV
η_{anode}	1.42E-10	mV
$\eta_{cathode}$	2.42E-10	mV
$\eta_{conc.}$	-2.48E-03	mV
η_{ohm}	3.20E-03	mV
ΔV	0.812	V
I	1484.6	kA
P_{DC}	1.206	MW
P_{AC}	1.061	MW

Table B.4: Mass balance to the Pre-Reformer.

Stream		PRE-REF	REF-OUT
Phase	-	Vapor Phase	Vapor Phase
Temperature	ºC	850	850
Pressure	bar	1,12	1,1
Mass Flows	kg/hr	628,3	628,3
H2O	kg/hr	275,9	261,0
CH4	kg/hr	53,58	47,54
CO	kg/hr	45,52	68,623
H2	kg/hr	16,57	21,05
CO2	kg/hr	140,9	140,9
N2	kg/hr	-	-
O2	kg/hr	-	-
C2H6	kg/hr	38,59	34,33
C3H8	kg/hr	57,33	54,81

Table B.5: Mass balance to the Anode.

Stream		O2	PRE-ANOD	ANODE1
Phase	-	Vapor Phase	Vapor Phase	Vapor Phase
Temperature	ºC	850	850	850
Pressure	bar	1,12	1,1	1,1
Mass Flows	kg/hr	443,10	628,3	1071
H2O	kg/hr	-	261,0	481,1
CH4	kg/hr	-	47,54	0,00464
CO	kg/hr	-	68,63	137,9
H2	kg/hr	-	21,05	25,29
CO2	kg/hr	-	140,9	427,0
N2	kg/hr	-	-	-
O2	kg/hr	443,10	-	-
C	kg/hr	-	-	-
C2H6	kg/hr	-	34,33	-
C3H8	kg/hr	-	54,81	-

Table B.6: Mass balance to the Cathode.

Stream		AIR-HOT	AIR-OUT	O2
Phase	-	Vapor Phase	Vapor Phase	Vapor Phase
Temperature	C	850	850	850
Pressure	bar	1,12	1,12	1,12
Mass Flows	kg/hr	6341	5898	443,1
H2O	kg/hr	-	-	-
CH4	kg/hr	-	-	-
CO	kg/hr	-	-	-
H2	kg/hr	-	-	-
CO2	kg/hr	-	-	-
N2	kg/hr	4864	4864	-
O2	kg/hr	1477	1034	443,1
C	kg/hr	-	-	-
C2H6	kg/hr	-	-	-
C3H8	kg/hr	-	-	-

Table B.7: Mass balance to the Water Gas Shift Reactor.

Stream		ANODE5	ANODE 6
Phase	-	Vapor Phase	Vapor Phase
Temperature	C	300	300
Pressure	bar	1,1	1,1
Mass Flows	kg/hr	717,8	717,8
H2O	kg/hr	322,4	266,2
CH4	kg/hr	-	-
CO	kg/hr	92,4	5,1
H2	kg/hr	16,9	23,2
CO2	kg/hr	286,1	423,3
N2	kg/hr	-	-
O2	kg/hr	-	-
C	kg/hr	-	-
C2H6	kg/hr	-	-
C3H8	kg/hr	-	-

Table B.8: Mass balance to the PSA (streams ”H2” and ”H2-2” are not included in the mass balance to the PSA, they were only presented to demonstrate the outlet conditions of the CHHP system).

Stream		ANODEMIX	H2-1	TAILGAS	H2	H2-2
Phase	-	Vapor Phase	Vapor Phase	Vapor Phase	Vapor Phase	Vapor Phase
Temperature	C	18,8	18,8	18,8	18,8	18,8
Pressure	bar	17,7	17,7	17,7	17,7	17,7
Mass Flows	kg/hr	473,9	38,2	435,7	16,5	21,7
H2O	kg/hr	0,6	-	0,6	-	-
CH4	kg/hr	-	-	-	-	-
CO	kg/hr	5,1	0,0	5,1	-	-
H2	kg/hr	44,9	38,2	6,7	16,5	21,7
CO2	kg/hr	423,3	-	423,3	-	-
N2	kg/hr	-	-	-	-	-
O2	kg/hr	-	-	-	-	-
C	kg/hr	-	-	-	-	-
C2H6	kg/hr	-	-	-	-	-
C3H8	kg/hr	-	-	-	-	-

Appendix C

Economic Analysis

Table C.1: Equipment cost for the main components on the CHHP system.

	Equipment Cost (M$)	So	S	CEPCIo	CEPCI (2019)	Cost without installation (M$)	IF	Installation Cost (M$)
SOFC[1]	4.268			550.8	607.5	4.707	1.00	4.001
Reformer[2]	0.204	1 125	396	521.9	607.5	0.114	1.10	0.107
WGS reactor [2]	0.169	1 500	396	521.9	607.5	0.077	1.10	0.072
Heat exchangers[3]	0.952					0.952	1.00	0.809
Multi-stage compressor [4]	0.329			390.4	607.5	0.512	1.20	0.615
PSA [5]	0.336			567.3	607.5	0.360	1.20	0.367
Total								5.971

Table C.2: SOFC modelling for the 1.744 MW CHHP system.

Parameter	Value	Units
$\triangle V$	0.822	V
I	2412	kA
P_{DC}	1.982	MW
P_{AC}	1.744	MW
H_2 production	19.2	kg/h
H_2 production	462	kg/day

[1] Installed SOFC cost: 4 000 $/kW [109].

[2] SMR derived H_2 case study. Scaled based on kg H_2/day produced [105].

[3] AspenTech Economic Analyzer Software.

[4] Online Equipment Cost Estimator. Power consumption provided by Aspen Plus and Stainless Steel as the chosen material[139].

[5] Uninstalled PSA cost: 315$/kW [113].

Table C.3: Total Investment costs regarding the 1.744 MW CHHP system.

	Cost (M€)
Base Equipment (BE)	8.60
Direct Costs	14.02
Indirect Costs	6.03
Total Investment	20.05

Table C.4: Average cost for the components used in the CHHP system.

Component	**Average Cost**	**Source/Units**
Fuel Gas	0.0191	Galp (€/kWh)
Hydrogen	12.0	€/kg
Electrical Energy (Purchase Cost)	0,100	Galp (€/kWh)
Heat	4.37	€/MMBtu

Table C.5: Operational costs and profit for the scenario with a payback of 3 years and 2 months (from year 1 to year 10).

	Year 1	Year 2	Year 3	Year 4	Year 5	Year 6	Year 7	Year 8	Year 9	Year 10
Operational Costs (M€)	0.813	0.813	0.813	7.905	0.813	0.813	0.813	0.813	0.813	7.905
Profit (M€)	9.309	9.309	9.309	9.309	9.309	9.309	9.309	9.309	9.309	9.309
Revenue (M€)	-18.75	-10.26	-1.759	6.737	1.404	8.496	8.496	8.496	8.496	1.404

Table C.6: Operational costs and profit for the scenario with a payback of 3 years and 2 months (from year 11 to year 20).

	Year 11	Year 12	Year 13	Year 14	Year 15	Year 16	Year 17	Year 18	Year 19	Year 20
Operational Costs (M€)	0.813	0.813	0.813	0.813	7.905	0.813	0.813	0.813	0.813	0.813
Profit (M€)	9.309	9.309	9.309	9.309	9.309	9.309	9.309	9.309	9.309	9.309
Revenue (M€)	8.496	8.496	8.496	8.496	1.404	8.496	8.496	8.496	8.496	8.496

Table C.7: Operational costs and profit for the scenario with a payback of 3 years and 6 months (from year 1 to year 10).

	Year 1	Year 2	Year 3	Year 4	Year 5	Year 6	Year 7	Year 8	Year 9	Year 10
Operational Costs (M€)	0.741	0.741	0.741	0.741	7.705	0.741	0.741	0.741	0.741	7.705
Profit (M€)	7.699	7.699	7.699	7.699	7.699	7.699	7.699	7.699	7.699	7.699
Revenue (M€)	-18.040	-11.083	-4.125	2.832	-0.0065	6.957	6.957	6.957	6.957	-0.0065

Table C.8: Operational costs and profit for the scenario with a payback of 3 years and 6 months (from year 11 to year 20).

	Year 11	Year 12	Year 13	Year 14	Year 15	Year 16	Year 17	Year 18	Year 19	Year 20
Operational Costs (M€)	0.741	0.741	0.741	0.741	7.705	0.741	0.741	0.741	0.741	0.741
Profit (M€)	7.699	7.699	7.699	7.699	7.699	7.699	7.699	7.699	7.699	7.699
Revenue (M€)	6.957	6.957	6.957	6.957	-0.0065	6.957	6.957	6.957	6.957	6.957

Table C.9: Input parameters and SOFC modelling for the scenario with a payback of 3 years and 2 months.

	Value	Units
Fuel gas	22.5	kmol h^{-1}
Air	352.1	kmol h^{-1}
Fresh water	19.5	kmol h^{-1}
Δ V	0.836	V
I	2412	kA
P DC	2.015	MW
P AC	1.773	MW
H_2 production	70.1	kg h^{-1}
H_2 production	1 682	kg day^{-1}